Wave Reflections in a Semi-infinitely Long Cylinder with an Attached Solid of Revolution

by

Nairui Yin

A Thesis submitted to the Faculty of Graduate Studies
in partial fulfillment of the requirements for the
Master of Science in Engineering Degree in
Control Engineering

Lakehead University

June, 2008

Your file Votre référence
ISBN: 978-0-494-43438-3
Our file Notre référence
ISBN: 978-0-494-43438-3

Abstract

A numerical procedure is presented for the study of end reflections in a semi-infinitely long isotropic circular cylinder with attached piezoelectric patch. The hybrid method which combines the finite element formulation in the piezoelectric patch with a wave function expansion representation in the isotropic cylinder is employed in the study. The global solution is obtained by imposing the continuity conditions on the displacements and tractions at the interface between the piezoelectric patch and the cylinder.

To obtain the wave functions in the cylinder, the governing equations of the cylinder are discretized by a semi-analytical finite element formulation where the discretization occurs through the cylinder's thickness. Solutions in the cylinder are constructed with modal data from a spectral decomposition of the differential equations governing its natural vibrations. These modal data consist of all propagating modes and edge vibrations, constituting the basis for a wave function expansion of the reflection of waves arriving at the end of the cylinder. On the other hand, the piezoelectric patch is discretized by the axisymmetric finite element formulation. Both least-square and virtual work methods are used for evaluating the amplitudes of the reflected wave field.

A computer code is developed in the study. Numerical cases are presented to demonstrate the effectiveness and accuracy of the code. The reflections due to monochromatic incoming axisymmetric and flexural wave are studied. For an oscillating end voltage that is out-of-phase with the incoming wave, it is possible to extract electrical energy which is called as energy harvesting. By applying appropriate voltage in the piezoelectric patch, the reflected propagating waves in the cylinder can be eliminated efficiently which is called as passive-control. Cases of such an

oscillating voltage with a particular radial distribution are given. Results presented in this study are for different thickness of piezoelectric patch, boundary condition and distribution of applied voltage. The results illustrate the amount of extracted energy as a function of the frequency of the incident monochromatic wave. The study has potential to apply in NDE (nondestructive evaluation), energy harvest and USM (ultrasonic motor).

Acknowledgement

I wish to sincerely thank most sincerely my supervisor, Prof. Hao Bai and co-supervisor Prof. Ke Fu Liu for their continuous guidance, encouragement and understanding throughout this project. In the same time, I would specially thank Prof. Xiao Ping Liu for his help in study and research.

I would like to thank my friends Ming Gong, Jerry Huang, Xi Jiang Dou, Yin He, Wen Guang Li and Huasu Su for their support and inspiration in my life.

Finally, I would like to express my appreciation to my parents. They help me overcome difficulty in life. In particular, my wife Juan Sun gave me many supports to finish this research work.

Table of Contents

List of Figures

List of Tables

List of Cases

List of Notations

r, θ, z	radial, circumferential and axial directions
u_r, u_θ, u_z	components of mechanical displacement
$T_{rr}, T_{\theta\theta}, T_{zz}, T_{\theta z}, T_{rz}, T_{r\theta}$	components of mechanical stress
$S_{rr}, S_{\theta\theta}, S_{zz}, S_{\theta z}, S_{rz}, S_{r\theta}$	components of mechanical strain
D_r, D_θ, D_z	components of electric displacement
E_r, E_θ, E_z	components of electric field
ϕ	electric potential
f_r, f_θ, f_z	components of body force
[C]	matrices of elastic anisotropic moduli
[e]	matrices of piezoelectric constants
[ε]	matrices of dielectric permittivities
$[\mathbf{C}^*]$	matrix representing conglomeration of **[C]**, **[e]** and [ε]
c^0	elastic modulus
e^0	piezoelectric constant
ρ^0	mass density
ε^0	dielectric constant
E^0	electric field constant
[L]	the differential operator
H	cylinder thickness
ω	the normalized circular frequency
k_m, m	the axial and circumferential wave numbers
$[K_1], [K_2], [K_3]$	stiffness matrices
$[K_4], [K_5], [K_6]$	
$[M]$	mass matrix
$\{\mathbf{t}_n\}$	the nodal stress of the nth mode
$\{\mathbf{p}_n\}$	the nodal electric potential of the nth mode

$\{\mathbf{d}_n\}$	the nodal electric displacement of the nth mode
$\{\mathbf{u}_n\}$	the nodal mechanical displacement of the nth mode
$[N_e]$	the finite element interpolation matrix
$\{\mathbf{v}_e\}$	the field variables of nodal displacement and electric potential
$\{\mathbf{V}_e\}$	the nodal displacement and electric potential in an element
$\{\mathbf{V}_0\}$	the modal distribution of mechanical displacements and electric potential
$\{\mathbf{F}_0\}$	the modal distribution of force and electric displacement
$\{\mathbf{F}_I\}$, $\{\tilde{\mathbf{F}}_B\}$	the nodal forces and electric displacements in interior areas of piezoelectric patch and in the interface
$\{\mathbf{V}_I\}$, $\{\tilde{\mathbf{V}}_B\}$	the nodal displacements and electric potential in interior areas of piezoelectric patch and in the interface
$\{\mathbf{V}^s\}$	reflected wave field
R_j	the reflection coefficient of the jth wave mode
$\{\mathbf{V}_B^{in}\}$	the nodal displacements and electric potential corresponding to the incident wave traveling
$\{\mathbf{F}_B^{in}\}$	the nodal force and electric displacement corresponding to the incident wave traveling
$\{\mathbf{V}_B^s\}$	the nodal displacements and electric potentials of scattering waves in interface
$\{\mathbf{F}_B^s\}$	the nodal forces and electric displacements of scattering waves in interface
E_n	the energy carried by the nth propagating mode

E_{in}	the input energy
E_{out}	the outgoing energy
$v_1(r), v_2(r), v_3(r)$	the distribution of applied voltage in the radial direction
r_i	the inner radius of the cylinder
r_o	the outer radius of the cylinder
L	thickness of the piezoelectric patch
c_1, c_2	the longitudinal wave and torsional wave velocities
ν	Poisson's ratio
$\{\mathbf{Q}^{in}\}$	distributions of forces and electric displacements stimulated by given incident wave
$\{\mathbf{Q}^{\phi}\}$	distributions of forces and electric displacements stimulated by oscillating end voltage
ϕ_0	normalized magnitude of applied voltage

Chapter 1 Introduction

1.1 Background

Nondestructive evaluation (NDE) is a specialized technical inspection method. NDE examines actual production pieces and reveals the presence of flaws without impairing their future usefulness. Ultrasonic inspection uses instrumentation converts electrical pluses into mechanical vibrations. The traveling wave reflects from flaws. The reflected pulses can be reconverted to electrical energy that can be measured. Their timing and size determine the position and size of the flaws.

There is a surge research in the energy harvesting in this decade. The use of piezoelectric structure to capture ambient vibration and transform mechanical strain energy into electrical charge is one important development.

End resonance generated by applying voltage in the piezoelectric patch can be used to create new types of motor, namely ultrasonic motor (USM). Comparing with traditional electro-magnetic motor, USM has many advantages to realize small size.

In this study, transmitted problem of a semi-infinitely long cylinder with the piezoelectric patch is investigated and some performances are represented by numerical cases. It has potential to apply in NDE, energy harvest and USM.

1.2 Literature Review

1.2.1 Guided wave in cylinder

Pochhammer [1] found the axially symmetric, vibration solution for harmonic waves in an infinitely long, homogeneous, isotropic cylinder. The dispersion equation contained three variables (Poisson's ratio, the angular frequency, and propagation constant) in dimensionless form. The dispersion relation are derived from the equations of elastic motion and the boundary conditions for a traction-free surface.

Based on the linear theory of elasticity, the three-dimensional solution of a guided wave in an infinitely long, homogeneous, isotropic hollow cylinder was studied by Gazis [2] and Armenàkas *et al.* [3]. Their general solution did not need the assumption of axial symmetry.

Using Frobenius' method, Mirsky [4,5] obtained an exact, infinite power series solution for axisymmetric waves traveling in an infinitely long, orthotropic, solid and hollow cylinders. Based on the same method but somewhat a different solution procedure, Nowinski [6] obtained an exact, infinite power series solution for a longitudinal wave traveling in a homogeneous orthotropic solid cylinder of infinite extent. Further results on this subject can be found in Chou and Achenbach [7] and Armenàkas and Reitz [8].

1.2.2 Numerical method

A three-dimensional finite element formula based on the variational principles was established by EerNisse [9]. And similar research for piezoelectric structure was investigated by Allik and Hughes [10]. Nelson *et al.* [11] and Huang and Dong [12]

presented a stiffness method to study wave propagation in laminated anisotropic cylinders with an arbitrary number of lamina. In this method, the thickness of the cylinder is discretized as sub layers. The displacements in each sub layer are evaluated through the use of interpolation functions that involve displacements solely at interfaces between the sub layers and the middle of each sub layer as the generalized coordinate parameters. Following a similar numerical procedure, Rattanawangcharoen and Shah [13,14] considered the dispersion relation of laminated composite cylinders. George and John [15] used one-dimensional finite element method to solve axisymmetric vibration of infinite piezoelectric cylinders. The dependence upon θ, z, and time was included by assuming appropriate trigonometric functions and the *3-D* problem was reduced to a one-dimensional (*1-D*) finite element with four degrees of freedom per node. George and John [16] developed their work to anisotropic cylinders. The finite element was used to model the cross-section of the cylinder in r, θ coordinates. Material constants that were functions of θ were allowed to vary in each circular sector and were computed using standard tensor transformations.

1.2.3 End resonance

End resonance is manifested by large (but bounded) amplitude displacements at the end of the structure, and such a phenomenon takes place in a very narrow band-width. End resonance in isotropic circular cylinders was first found experimentally by Oliver [17] and determined by McNiven [18] analytically. This result was further improved by Zemanek [19] within 0.5% with nine modes. Naillon, Coursant and Besnier [20] examined the resonance phenomena of piezoelectric structures by using echo graphic probes. They compared the electric characteristics of parallel periodic rods observed experimentally to those determined using the finite element method. The work done by Ostergaard and Pawlak [21] explained the finite element model as implemented in ANSYS engineering analysis system theoretical manual. This model allowed for the

solution of the static and electro-elastic vibration of different piezoelectric devices. The least square method was employed in Gregory and Gladwell [22] for studying the axisymmetric waves in a semi-infinitely long, elastic rod. The rod was stimulated either by tractions acting over its end face or by a propagating mode reflected at a free end surface. Their work showed that the end resonance frequencies depend strongly on the Poisson ratio. Kharouf and Heyliger [23] developed Ritz method with elements of power series and Fourier series to solve frequency problem for piezoelectric cylinders. Good agreement was obtained with results reported from the literature of frequencies, displacements and electric potential. Taweel *et al.* [24] explored the reflected wave field in a semi-infinitely long laminated composite cylinder with a general cross-section. Using numerical computation, end resonances for semi-infinite piezoelectric cylinders were determined carefully by Bai *et al.* [25].

1.2.4 Energy harvest

When appropriate voltage is applied to the end of piezoelectric patch, energy carried by reflected waves can be optimized to a minimal value. Part of incoming wave energy is extracted by electric field through the end of piezoelectric patch. This phenomenon is called as energy harvest. There is a great mount of literature on energy harvest in the last decade. Umeda *et al.* [26] made an investigation of the fundamentals of a generator, which transformed mechanical energy to electrical energy using a piezoelectric vibrator and a steel ball. The calculated output voltage is close to results in experiments. Some suggestions for optimizing transform proportion were given. Cornwell and Goethal [27] used auxiliary structures, consisting of a mechanical fixture and a piezoelectric element to tune the vibration system for higher energy harvest. By adjusting various parameters of these structures, the strain induced in the attached PZT element can be maximized and power output is improved. Bai *et al.* [25] discussed energy harvest in a semi-infinite piezoelectric cylinder for an incoming chromatic wave. The optimizing method of adjusting boundary electrical

condition was given by minimizing reflection energy.

1.3 Objectives

1. The frequency spectra of thick and thin isotropic cylinders were investigated by using the semi-analytic finite element method.

2. End resonance and energy harvest for a semi-infinitely long cylinder with a piezoelectric patch were investigated. The corresponding optimized applied voltage distributions which minimized the outgoing energy were given.

3. Different circumferential wave numbers (m = 0 and m = 1) were considered and 'backward waves' were found in certain range of normalized circular frequency when $m = 0$.

4. Results with grounded and open circuit conditions at the end of the piezoelectric patch were compared.

1.4 Organization of the Thesis

This thesis focuses on the investigation of the propagating and scattering of guided wave in semi-infinite cylinders with piezoelectric patch. Introduction and literature review are presented in Chapter 1. A semi-analytical formulation for wave propagation in a cylinder is discussed in Chapter 2. Two kinds of eigenvalue problems are studied, the dispersion relations are given and frequency spectra for the thick and thin cylinders are plotted by solving the first kind eigenvalue problem. In Chapter 3, a hybrid finite element method is employed to study wave scattering problem in a semi-infinitely long cylinder attached piezoelectric patch. The piezoelectric patch is discretized by the axisymmetric element and the semi-infinite cylinder is modeled by

a wave function expansion. The continuity conditions at the interface are enforced to form the global equations of motion of the system. Numerical results are presented. End resonance is observed for circumferential wave $m = 0$ for both thick and thin cylinders. Energy harvest is carefully studied. Finally, conclusions and recommendation are given in the Chapter 4.

Chapter 2 Guided wave in a Cylinder

The study of wave propagation in a cylindrical structure is important for the non-destructive testing of flaws. In this chapter, the Hamilton principle is applied to arrive at equations of motion for the piezoelectric cylinder and isotropic cylinder. By using semi-analytical FEM method in the radial direction, wave form solutions of wave forms and frequency spectra of the cylinder can be obtained.

2.1 Equations of motion

For a circular cylinder, cylindrical coordinates and Cady's notation (1964) are used to represent the field variables. The primary dependent variables are: mechanical displacement $\{\mathbf{u}\} = [u_r, u_\theta, u_z]^T$; stress $\{\mathbf{T}\} = [T_{rr}, T_{\theta\theta}, T_{zz}, T_{\theta z}, T_{rz}, T_{r\theta}]^T$; strain $\{\mathbf{S}\} = [S_{rr}, S_{\theta\theta}, S_{zz}, S_{\theta z}, S_{rz}, S_{r\theta}]^T$; electric displacement $\{\mathbf{D}\}=[D_r, D_\theta, D_z]^T$; electric field $\{\mathbf{E}\} = [E_r, E_\theta, E_z]^T$; electric potential ϕ, and body force $\{\mathbf{f}\} = [f_r, f_\theta, f_z]^T$. Properties of isotropic elastic material can be represented by setting electric displacement $\{\mathbf{D}\}$ and electric field $\{\mathbf{E}\}$ as zero.

2.1.1 Normalization

Because of larger difference between the materials quoted in their usual units, non-dimensional method is applied to circumvent numerical anomalies. In equation (2.1), below quantities on the right-hand and left-hand sides of the equations are presented in their respective dimensional and dimensionless forms. Four key parameters are needed: (1) cylinder thickness H, (2) an elastic modulus c^0, (3) a piezoelectric constant e^0, and (4) mass density ρ^0, dielectric constant ε^0 and electric

field E^0 can be defined as: $\varepsilon^0 = \left(e^0\right)^2 / c^0$ and $E^0 = c^0 / e^0$. The other independent and dependent variables and material properties are normalized as

$$
\begin{aligned}
&r = \frac{r}{H}, \quad z = \frac{z}{H}, \quad t = \frac{t}{H}\sqrt{\frac{c^0}{\rho^0}}, \\
&u_i = \frac{u_i}{H} \quad (i = r,\theta,z), \quad T_p = \frac{T_p}{c^0}, \quad S_p = S_p \quad (p = 1,2,...,6), \\
&D_k = \frac{D_k}{e^0}, \quad E_k = \frac{E_k}{E^0} \quad (k = 1,2,3), \\
&c_{pq} = \frac{c_{pq}}{c^0}, \quad \varepsilon_{ij} = \frac{\varepsilon_{ij}}{\varepsilon^0}, \quad \mathrm{e}_{ip} = \frac{\mathrm{e}_{ip}}{e^0}, \quad \rho_i = \frac{\rho_i}{\rho^0} \quad (p,q = 1,2,...,6), \\
&\rho_e = \frac{H\rho_e}{e^0}, \quad f_i = \frac{Hf_i}{c^0} \quad (i = r,\theta,z).
\end{aligned}
\tag{2.1}
$$

2.1.2 Equations of motion

In the cylindrical coordinate system, equations of motion for a piezoelectric cylinder are given by

$$
\begin{aligned}
&\frac{\partial T_{rr}}{\partial r} + \frac{1}{r}\frac{\partial T_{r\theta}}{\partial \theta} + \frac{\partial T_{rz}}{\partial z} + \frac{T_{rr} - T_{\theta\theta}}{r} + f_r = \rho\ddot{u}_r, \\
&\frac{\partial T_{\theta r}}{\partial r} + \frac{1}{r}\frac{\partial T_{\theta\theta}}{\partial \theta} + \frac{\partial T_{\theta z}}{\partial z} + 2\frac{T_{r\theta}}{r} + f_\theta = \rho\ddot{u}_\theta, \\
&\frac{\partial T_{zr}}{\partial r} + \frac{1}{r}\frac{\partial T_{z\theta}}{\partial \theta} + \frac{\partial T_{zz}}{\partial z} + \frac{T_{rz}}{r} + f_z = \rho\ddot{u}_z, \\
&\frac{\partial D_r}{\partial r} + \frac{1}{r}\frac{\partial D_\theta}{\partial \theta} + \frac{\partial D_z}{\partial z} = 0.
\end{aligned}
\tag{2.2}
$$

2.1.3 Hooke's law

The general Hooke's law for piezoelectric properties is given as follows

$$\{\mathbf{Q}\} = \left[\mathbf{C}^*\right]\{\mathbf{q}\} \tag{2.3}$$

where

$$\left[\mathbf{C}^*\right] = \begin{bmatrix} \mathbf{C} & -\mathbf{e}^T \\ \mathbf{e} & \boldsymbol{\varepsilon} \end{bmatrix}_{9\times 9}, \quad \{\mathbf{Q}\} = \begin{Bmatrix} \mathbf{T} \\ \mathbf{D} \end{Bmatrix}_{9\times 1}, \quad \{\mathbf{q}\} = \begin{Bmatrix} \mathbf{S} \\ \mathbf{E} \end{Bmatrix}_{9\times 1},$$

and [**C**], [**e**] and [**ε**] are matrices of elastic anisotropic moduli (6×6), piezoelectric constants (6×3) and dielectric permittivities (3×3), respectively, with $[\mathbf{C}^*]$ being a (9× 9) matrix representing their conglomeration.

2.1.4 Generalized strain-displacement relations

Generalized strain-displacement relations in cylindrical coordinate are given by

$$\begin{aligned}
S_{rr} &= \frac{\partial u_r}{\partial r}, & S_{\theta\theta} &= \frac{1}{r}\frac{\partial u_\theta}{\partial \theta} + \frac{u_r}{r}, \\
S_{zz} &= \frac{\partial u_z}{\partial z}, & S_{\theta z} &= \frac{\partial u_\theta}{\partial z} + \frac{1}{r}\frac{\partial u_z}{\partial \theta}, \\
S_{rz} &= \frac{\partial u_z}{\partial r} + \frac{\partial u_r}{\partial z}, & S_{r\theta} &= \frac{1}{r}\frac{\partial u_r}{\partial \theta} + \frac{\partial u_\theta}{\partial r} - \frac{u_\theta}{r}, \\
E_r &= -\frac{\partial \phi}{\partial r}, & E_\theta &= -\frac{1}{r}\frac{\partial \phi}{\partial \theta}, & E_z &= -\frac{\partial \phi}{\partial z}.
\end{aligned} \tag{2.4}$$

Above equation can be written in a compact form as

$$\{\mathbf{Q}\} = [\mathbf{L}]\{\mathbf{v}\}, \tag{2.5}$$

where $\{\mathbf{v}\} = \begin{bmatrix} u_r & u_\theta & u_z & \phi \end{bmatrix}^T$ and the differential operator [**L**] is given in the Appendix.

2.2 Semi-analytical FEM

In this section, the equivalent expression for equations of motion is given by using the Hamilton principle. Applying finite element method to discretize the cylinder in the radial direction and substituting wave form solution into discretized equations of motion, eigenvalue equations for the cylinder can be derived. Propagating and non-propagating waves can be distinguished by setting the axial wave numbers to different values.

2.2.1 Hamilton principle

Hamilton principle can be expressed as

$$\int_{t_0} \delta(K-H)\, dt + \int_{t_0} \delta W\, dt = 0, \tag{2.6}$$

where K, H and W are the kinetic energy, electric enthalpy and non-conservative energy, respectively.

The kinetic energy is given as

$$K = \frac{1}{2}\iiint_V \{\dot{\mathbf{v}}\}^T [\boldsymbol{\rho}]\{\dot{\mathbf{v}}\} dV, \tag{2.7}$$

where $$[\boldsymbol{\rho}] = \begin{bmatrix} \rho & & & \\ & \rho & & \\ & & \rho & \\ & & & 0 \end{bmatrix}.$$

Because of zero body and surface forces, the work done by non-conservative force is not involved in the present analysis, or $W = 0$.

The electric enthalpy, H, which represents the internal strain energy of an elastic medium, is given by

$$H = \frac{1}{2}\iiint_V \left(\{\mathbf{q}\}^T [\mathbf{C}^*]\{\mathbf{q}\} - \{\mathbf{E}\}^T \{\mathbf{D}\}\right) dV. \tag{2.8}$$

Substituting equation (2.3) into the above equation, a compact form of H is found to be

$$H = \frac{1}{2}\iiint_V \{\mathbf{q}\}^T \left[\mathbf{C}^{**}\right]\{\mathbf{q}\}dV\,, \tag{2.9}$$

where

$$\left[\mathbf{C}^{**}\right] = \begin{bmatrix} \mathbf{C} & -\mathbf{e}^T \\ -\mathbf{e} & -\boldsymbol{\varepsilon} \end{bmatrix}.$$

2.2.2 Quadratic element

The geometry, boundary force and material matrices of a semi-infinite cylinder are axisymmetric. Isoparametric finite-element methodology and numerical integration are used to discretize the cylinder in the radial direction.

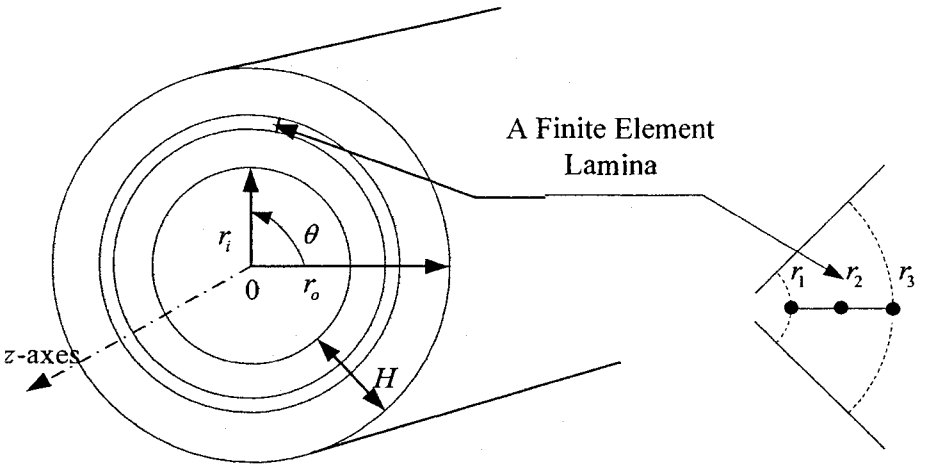

Figure 1. Cross section of a cylinder

The explicit interpolation forms of a three-node quadratic element in a physical element is given by

$$n_1(\xi) = \frac{1}{2}\xi(\xi-1)\,,\; n_2(\xi) = 1-\xi^2\,,\; n_3(\xi) = \frac{1}{2}\xi(\xi+1)\,, \tag{2.10}$$

where ξ is local variable $(-1 \le \xi \le +1)$.

According to the interpolation functions, the interpolations of the geometry and

any one of the field variables, say x, over the isoparametric element are given by

$$x = n_1(\xi)x_1 + n_2(\xi)x_2 + n_3(\xi)x_3 . \tag{2.11}$$

The field variables $\{\mathbf{v}_e\}$ in a three-node quadratic element can be written as

$$\{\mathbf{v}_e(r,\theta,z,t)\} = [N_e(\xi)]\{\mathbf{V}_e(\theta,z,t)\}, \tag{2.12}$$

where

$$[N_e(\xi)] = \begin{bmatrix} n_1(\xi) & n_2(\xi) & n_3(\xi) & & & & & & & & & \\ & & & n_1(\xi) & n_2(\xi) & n_3(\xi) & & & & & & \\ & & & & & & n_1(\xi) & n_2(\xi) & n_3(\xi) & & & \\ & & & & & & & & & n_1(\xi) & n_2(\xi) & n_3(\xi) \end{bmatrix},$$

and $\{\mathbf{V}_e\} = [\mathbf{v}_1 \ \mathbf{v}_2 \ \mathbf{v}_3]^T = [u_{1r} \ u_{2r} \ u_{3r} \ u_{1\theta} \ u_{2\theta} \ u_{3\theta} \ u_{1z} \ u_{2z} \ u_{3z} \ \phi_1 \ \phi_2 \ \phi_3]^T$,

here $[N_e(\xi)]$ means the finite element interpolation form and $\{\mathbf{V}_e\}$ denotes the vector of the nodal displacement and electric potential in a three-node quadratic element.

By assembling variables $\{\mathbf{v}_e\}$, $\{\mathbf{V}_e\}$ and matrices $[N_e(\xi)]$ of every three-node quadratic element in the cylinder, global variables $\{\mathbf{v}\}$, $\{\mathbf{V}\}$ can be denoted as

$$\{\mathbf{v}(r,\theta,z,t)\} = [N(\xi)]\{\mathbf{V}(\theta,z,t)\}, \tag{2.13}$$

where $[N(\xi)]$ means the finite element interpolation over the whole cylinder.

Substituting equation (2.12) into equation (2.5), the general strain-displacement relations in the whole cylinder can be written as

$$\begin{aligned} \{\mathbf{q}\} &= [\mathbf{L}]\{\mathbf{v}\} = [\mathbf{L}]([N(\xi)]\{\mathbf{V}\}) \\ &= [\mathbf{L}_r]([N(\xi)]\{\mathbf{V}\}) + [\mathbf{L}_\theta]([N(\xi)]\{\mathbf{V}\}) + [\mathbf{L}_z]([N(\xi)]\{\mathbf{V}\}) \\ &= [B_1]\{\mathbf{V}\} + [B_2]\{\mathbf{V}_{,\theta}\} + [B_3]\{\mathbf{V}_{,z}\} \end{aligned}, \tag{2.14}$$

where $\{\mathbf{V}_{,\theta}\} = \dfrac{\partial\{\mathbf{V}\}}{\partial\theta}$, $\{\mathbf{V}_{,z}\} = \dfrac{\partial\{\mathbf{V}\}}{\partial z}$. Differential operators $[\mathbf{L}_r]$, $[\mathbf{L}_\theta]$, $[\mathbf{L}_z]$ and the matrices $[B_1]$, $[B_2]$, $[B_3]$ are given in Appendix.

Substituting equation (2.14) into equation (2.9), the latter becomes

$$\int_{t_0}^{t} \delta L dt + \int_{t_0}^{t} \delta W dt = \delta \int_{t_0}^{t} dt \iint \frac{1}{2}(\{\dot{\mathbf{V}}\}^T [\mathrm{M}]\{\dot{\mathbf{V}}\} - \{\mathbf{V}\}^T [K_{11}]\{\mathbf{V}\} - \{\mathbf{V}\}^T [K_{12}]\{\mathbf{V}_{,\theta}\}$$
$$-\{\mathbf{V}\}^T [K_{13}]\{\mathbf{V}_{,z}\} - \{\mathbf{V}_{,\theta}\}^T [K_{21}]\{\mathbf{V}\} - \{\mathbf{V}_{,\theta}\}^T [K_{22}]\{\mathbf{V}_{,\theta}\} - \{\mathbf{V}_{,\theta}\}^T [K_{23}]\{\mathbf{V}_{,z}\} \quad , (2.15)$$
$$-\{\mathbf{V}_{,z}\}^T [K_{31}]\{\mathbf{V}\} - \{\mathbf{V}_{,z}\}^T [K_{32}]\{\mathbf{V}_{,\theta}\} - \{\mathbf{V}_{,z}\}^T [K_{33}]\{\mathbf{V}_{,z}\}) d\theta dz = 0$$

where

$$[K_{11}] = \int [B_1]^T [\mathbf{C}^{**}][B_1] r\, dr\,, \quad [K_{12}] = \int [B_1]^T [\mathbf{C}^{**}][B_2] r\, dr\,,$$
$$[K_{13}] = \int [B_1]^T [\mathbf{C}^{**}][B_3] r\, dr\,, \quad [K_{21}] = \int [B_2]^T [\mathbf{C}^{**}][B_1] r\, dr\,,$$
$$[K_{22}] = \int [B_2]^T [\mathbf{C}^{**}][B_2] r\, dr\,, \quad [K_{23}] = \int [B_2]^T [\mathbf{C}^{**}][B_3] r\, dr\,,$$
$$[K_{31}] = \int [B_3]^T [\mathbf{C}^{**}][B_1] r\, dr\,, \quad [K_{32}] = \int [B_3]^T [\mathbf{C}^{**}][B_2] r\, dr\,,$$
$$[K_{33}] = \int [B_3]^T [\mathbf{C}^{**}][B_3] r\, dr\,, \quad [M] = \int [N_e]^T [\boldsymbol{\rho}][N_e] r\, dr,$$

here note that all integrals have lower and upper limits of inner radius r_i and outer radius r_o, respectively.

Finally, equations of motion can be given by

$$[K_1]\{\mathbf{V}\} + [K_2]\{\mathbf{V}_{,\theta}\} + [K_3]\{\mathbf{V}_{,z}\} - [K_4]\{\mathbf{V}_{,\theta\theta}\} - [K_5]\{\mathbf{V}_{,\theta z}\} - [K_6]\{\mathbf{V}_{,zz}\} + [M]\{\ddot{\mathbf{V}}\} = \{\mathbf{F}\}, \quad (2.16)$$

where $\{\mathbf{F}\}$ is nodal force vector and

$$[K_1]=[K_{11}]\,, \quad [K_2]=[K_{12}]-[K_{21}],$$
$$[K_4]=[K_{22}]\,, \quad [K_3]=[K_{13}]-[K_{31}],$$
$$[K_6]=[K_{33}]\,, \quad [K_5]=[K_{23}]+[K_{32}].$$

Note that $[K_1]$, $[K_4]$, $[K_5]$ and $[K_6]$ are symmetric while $[K_2]$ and $[K_3]$ are skew-symmetric.

2.2.3 Wave form solution

The wave form solution for harmonic motion in a cylinder can be given by

$$\{\mathbf{V}\} = \{\mathbf{V}_0\} e^{i(k_m z + m\theta - \omega t)}, \quad (2.17)$$

where ω is the normalized circular frequency, (k_m, m) are the axial and circumferential wave numbers, and $\{\mathbf{V}_0\}$ is the vector of the radial modal distribution of the displacement and electric potential.

Substituting equation (2.17) into equation (2.16), the following algebraic equation is obtained by

$$([K_1]+im[K_2]+ik_m[K_3]+m^2[K_4]+mk_m[K_5]+k_m^2[K_6])\{\mathbf{V}_0\}=\omega^2[M]\{\mathbf{V}_0\} \quad (2.18)$$

The algebraic equation can be transformed to two kinds of eigenproblem by assigning ω^2 or k_m as the eigenvalue.

2.2.4 Eigenproblem

Eigenvalue problem I:

With k_m assigned a certain value and ω^2 as eigenvalue, equation (2.18) becomes

$$[K]\{\mathbf{V}_0\}=\omega^2[M]\{\mathbf{V}_0\}, \quad (2.19)$$

where $[K]=[K_1]+im[K_2]+ik_m[K_3]+m^2[K_4]+mk_m[K_5]+k_m^2[K_6]$,

here the circumferential wave number m is assigned an integer to assure circumferential periodicity. Axial wave number k_m and circumferential wave number m are regarded as constants in this equation. For non-trivial solution $\{\mathbf{V}_0\}$, the determinant of $[K]$ must be zero. Since $[K]$ is a Hermitian matrix, only real ω^2 is admitted. Frequency spectra can be plotted by letting k_m be x-axis and positive real ω be y-axis.

Eigenvalue problem II:

By assigning ω^2, the eigenproblem can be transformed as

$$[A_1 - k_m B_1]\begin{Bmatrix} \mathbf{V}_0 \\ k_m \mathbf{V}_0 \end{Bmatrix} = 0. \tag{2.20}$$

where

$$[A_1] = \begin{bmatrix} 0 & I \\ -\left(K_1 + m^2 K_4 - \omega^2 M + imK_2\right) & -\left(mK_5 + iK_3\right) \end{bmatrix}, [B_1] = \begin{bmatrix} I & 0 \\ 0 & K_6 \end{bmatrix}.$$

Now, normalized circular frequency ω and circumferential wave number m are assigned as constants. For a non-trivial solution of the nodal displacements and electric potentials $\{\mathbf{V}_0\}$, the determinant of $[A_1\text{-}k_m B_1]$ must vanish. On the other hand, the eigenvector corresponding to the nth eigenvalue k_m represents the nodal displacements and electric potentials of the nth mode. By using strain-displacement relations, strain-stress relations and equivalent nodal force equations, the nodal forces and electric displacements of the nth mode can be derived. Introducing notations $\{\mathbf{t}_n\}$, $\{\mathbf{p}_n\}$, $\{\mathbf{d}_n\}$ and $\{\mathbf{u}_n\}$ as follows:

$$\begin{aligned}
\{\mathbf{t}_n\} &= \left[T_{zz,1\text{-}1,n},\ T_{z\theta,1\text{-}1,n},\ T_{zr,1\text{-}1,n},\ T_{zz,1\text{-}2,n},\ \cdots\ T_{zz,NE\text{-}3,n},\ T_{z\theta,NE\text{-}3,n},\ T_{zr,NE\text{-}3,n}\right]^T, \\
\{\mathbf{p}_n\} &= \left[\phi_{1\text{-}1,n},\ \phi_{1\text{-}2,n},\ \phi_{1\text{-}3,n},\ \phi_{2\text{-}1,n},\ \cdots\ \phi_{NE\text{-}2,n},\ \phi_{NE\text{-}3,n}\right]^T, \\
\{\mathbf{d}_n\} &= \left[D_{z,1\text{-}1,n},\ D_{z,1\text{-}2,n},\ D_{z,1\text{-}3,n},\ D_{z,2\text{-}1,n},\ \cdots\ D_{z,NE\text{-}2,n},\ D_{z,NE\text{-}3,n}\right]^T, \\
\{\mathbf{u}_n\} &= \left[u_{r,1\text{-}1,n},\ u_{\theta,1\text{-}1,n},\ u_{z,1\text{-}1,n},\ u_{r,1\text{-}2,n},\ \cdots\ u_{r,NE\text{-}3,n},\ u_{\theta,NE\text{-}3,n},\ u_{z,NE\text{-}3,n}\right]^T.
\end{aligned} \tag{2.21}$$

The subscripts are: (1) the first group, say zr, zz or $z\theta$, the traction and electrical displacement component, with the exception of ϕ which is a scalar, (2) the second group consists of two integers separated by a dash. They are the element number and the Guassian pointer within the element, respectively, NE stands for the total number of elements.

In a compact form, the nodal displacement and electric potential $\{\mathbf{V}_n\}$, the equivalent nodal forces and electric displacements $\{\mathbf{Q}_n\}$ of the nth mode are introduced as

$$\{\mathbf{V}_n\}=\begin{Bmatrix}\mathbf{u}_n\\ \mathbf{d}_n\end{Bmatrix},\quad \{\mathbf{Q}_n\}=\begin{Bmatrix}\mathbf{t}_n\\ \mathbf{p}_n\end{Bmatrix}. \tag{2.22}$$

The modal distribution of displacements and electric potentials [**G**], the modal distribution of forces and electric displacement [**F**] are given by

$$[\mathbf{G}]=[\mathbf{V}_1\quad \mathbf{V}_2\quad \cdots\quad \mathbf{V}_M],\quad [\mathbf{F}]=[\mathbf{F}_1\quad \mathbf{F}_2\quad \cdots\quad \mathbf{F}_M], \tag{2.23}$$

where $\{\mathbf{F}_i\}=\int_{r_i}^{r_o}\{\mathbf{Q}_i\}rdr$, and M is the total number of reflected modes.

Propagating and non-propagating waves can be distinguished by different value of the axial wave number k_m. Real k_m represents propagating waves, while the complex conjugate pairs represent non-propagating waves which is described as standing waves with spatially decaying amplitudes. Different signs of k_m mean different traveling direction of the wave. Herein the wave traveling from negative z-axis to positive z-axis is defined as the reflected wave and the wave with opposite traveling direction is defined as the incident wave. The relations of the wave characteristics and the normalized axial number k_m are summarized in Table 1.

Table 1. Wave with different values of k_m

k_m	$z>0$	$z<0$
Real	$k_m>0$ Propagating wave	$k_m<0$ Propagating wave
Complex	Imag(k_m)>0 Non-propagating wave	Imag(k_m)<0 Non-propagating wave

2.3 Energy flux

Since only propagating waves carry energy, the time-average value of the energy flux associated with the nth propagating mode is given by:

$$E_n = |a_n|^2 \omega \operatorname{Im}\left\{\left\langle\left\{\overline{\mathbf{t}_n}\right\},\left\{\overline{\mathbf{u}_n}\right\}\right\rangle + \left\langle\left\{\overline{\mathbf{d}_n}\right\},\left\{\overline{\mathbf{p}_n}\right\}\right\rangle\right\} = |a_n|^2 J_n, \tag{2.24}$$

where vectors $\{\mathbf{t}_n\}$, $\{\mathbf{u}_n\}$,$\{\mathbf{d}_n\}$ and $\{\mathbf{P}_n\}$ have been defined in equation (2.21), and

$$J_n = \omega \operatorname{Im}\left\{\left\langle\left\{\overline{\mathbf{t}_n}\right\},\left\{\overline{\mathbf{u}_n}\right\}\right\rangle + \left\langle\left\{\overline{\mathbf{d}_n}\right\},\left\{\overline{\mathbf{p}_n}\right\}\right\rangle\right\}.$$

The over bars denote complex conjugation, and

$$\langle \alpha, \beta \rangle = \int_{r_i}^{r_o} \alpha^H \beta r dr .$$

2.4 Numerical Studies

Two cases are presented herein to illustrate frequency spectra for infinitely long isotropic cylinders. In these cases, two different-sized cylinders (H/R = 1 and 0.135) are considered. They are identified as a thick cylinder (H/R = 1) and a thin one (H/R = 0.135). Here H is the thickness of the cylinder and R = $(r_i + r_o)/2$ is the mean radius.

In the numerical studies, H is taken as unit 1m for both cylinders. The inner and outer radii of the thick cylinder are r_i = 0.5 m and r_o = 1.5 m, respectively. The inner and outer radii of the thin cylinder are r_i = 6.9091 m and r_o = 7.9091 m, respectively.

The cylinder is made by steel. The longitudinal wave and torsional wave velocities are given, respectively, as

$$c_1 = 5.96 \times 10^3 \text{m/s}, \quad c_2 = 3.26 \times 10^3 \text{ m/s}.$$

The Young's modulus is 2.169×10^{11} Pa, the Poisson's ratio ν, mass density ρ, are $\nu = 0.287, \rho = 7.8 \times 10^3 \text{kg/m}^3$, respectively.

The normalized materials constants are

$$[C]=\begin{bmatrix} 3.3474 & 1.34742 & 1.34742 & . & . & . \\ 1.34742 & 3.3474 & 1.34742 & . & . & . \\ 1.34742 & 1.34742 & 3.3474 & . & . & . \\ . & . & . & 1 & . & . \\ . & . & . & . & 1 & . \\ . & . & . & . & . & 1 \end{bmatrix}_{6\times 6}$$

Based on given physical values, the normalized circular frequency is given by $\omega=\frac{\omega_{real}}{\omega_0}$, where $\omega_0=\frac{1}{H}\sqrt{c^0/\rho^0}$, c^0 is elastic constant and ρ^0 is mass density. For both cylinders, ω_0 is 1811.64 rad/s.

Case A

In the thick hollow cylinder, frequency spectra is plotted over the frequency range of interested $0< \omega <8.0$ for circumferential wave numbers $m = 0$ and $m = 1$, see Figure 2 through 4.

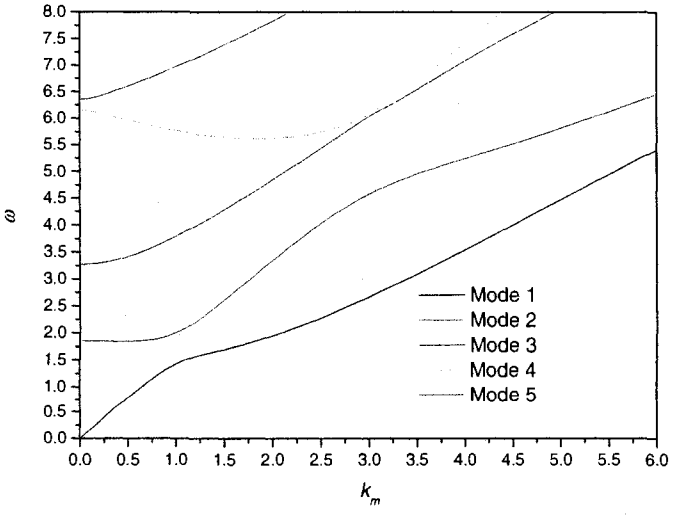

Figure 2. Frequency spectra for $m = 0$

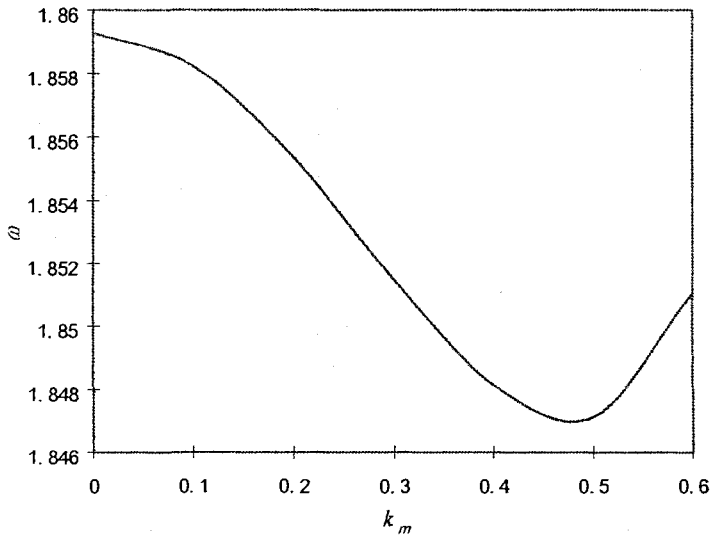

Figure 3. Backward wave for $m = 0$

For circumferential wave number $m = 0$, there are two cutoff frequencies ω = 1.859, ω = 3.271 when normalized circular frequency ω = 0.0-4.5. As shown in Figure 3, in the second branch there is a minimal value (ω = 1.847) when $k_m = 0.485$. Wave numbers k_m to the left of ω=1.847 are defined as "backward wave" , which travels in a negative group velocity.

There is one propagating wave when $0< \omega <1.847$, when $1.859< \omega <3.271$, two propagating waves exist, and three propagating waves exist when $3.271< \omega <4.5$. Otherwise, three propagating waves exist when $1.847< \omega <1.859$ because of 'backward wave'.

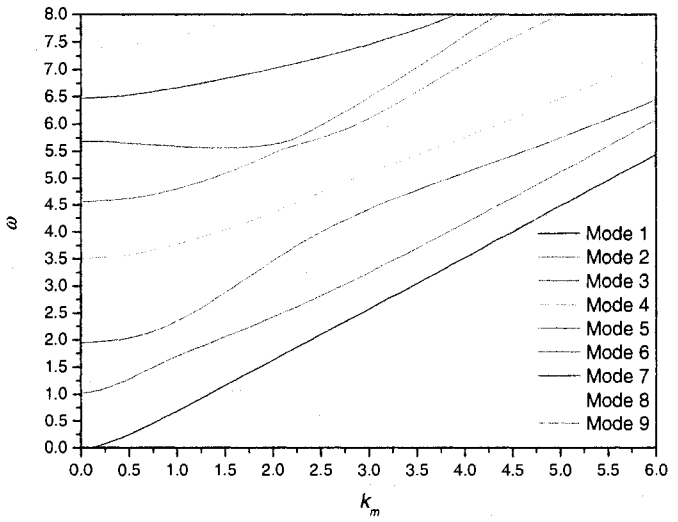

Figure 4. Frequency spectra for $m = 1$

As shown in Figure 4, for circumferential wave number $m = 1$, there are three cutoff frequencies $\omega = 1.027$, $\omega = 1.956$ and $\omega = 3.516$ at normalized circular frequency $\omega = 0.0\text{-}4.5$. No 'backward wave' is found when $0.0 < \omega < 4.5$.

Case B

For the thin cylinder, frequency spectra is plotted over the frequency range of consideration $0 < \omega < 8.0$ for circumferential wave numbers $m = 0$ and $m = 1$.

As shown in Figure 5, for circumferential wave number $m = 0$, there are two cutoff frequencies $\omega = 0.226$ and $\omega = 3.144$ at normalized circular frequency $\omega = 0.0\text{-}4.5$. By carefully searching no 'backward wave' is found at $\omega = 0.0\text{-}4.5$. The fourth branch has a 'backward wave'. However, it is beyond the frequency range of interest.

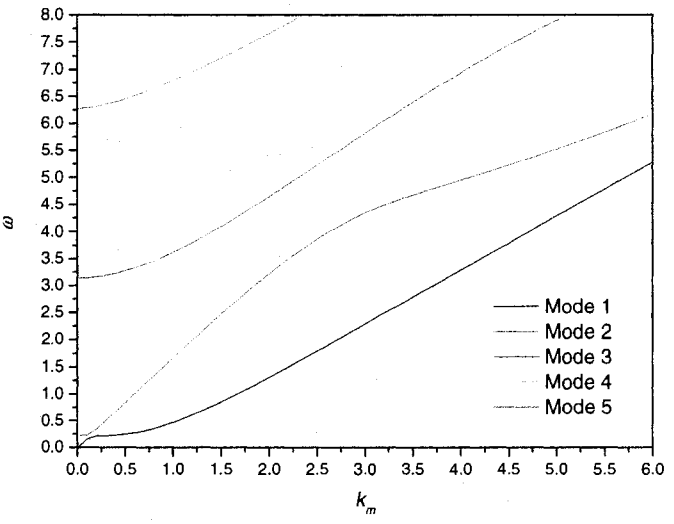

Figure 5. Frequency spectra for $m = 0$

As shown in Figure 6, for circumferential wave number m = 1, there are four cutoff frequencies ω = 0.135, ω = 0.319, ω = 3.147 and ω = 3.162 when $0 < \omega <$ 4.5. No backward wave exists in this frequency range. There is one propagating wave when $0 < \omega < 0.135$. Two propagating waves exist when $0.135 < \omega < 0.319$. Three propagating waves exist when $0.319 < \omega < 3.147$, four and five propagating waves exist respectively when $3.147 < \omega < 3.162$ and $3.162 < \omega < 4.5$.

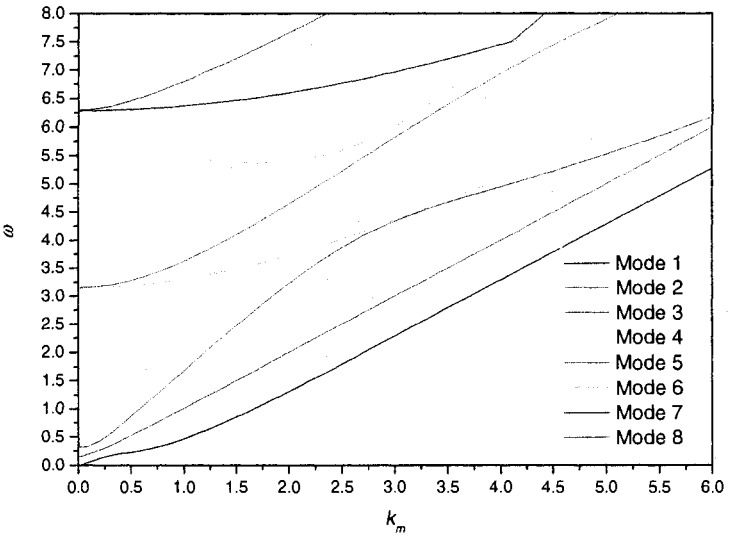

Figure 6. Frequency spectra for $m = 1$

Chapter 3 Wave Scattering in a Cylinder

3.1 Introduction

The model studied in this chapter, as shown in Figure 7, contains a semi-infinitely long, homogeneous cylinder and a piezoelectric patch. When an incident wave traveling from infinite along the negative z-direction strikes the interface of the cylinder and the piezoelectric patch, a scattering wave field is generated. The applied voltage or boundary force in the end of piezoelectric patch can affect the reflected and transmitted wave fields. A hybrid finite element and modal representation technique is applied herein to obtain the reflected wave field. In this method, the scattered wave field in the semi-infinitely long cylinder can be represented by a wave function expansion as studied in Chapter 2. On the other hand, the transmitted wave in the piezoelectric patch is modeled by an axisymmetric element. An eight-node quadratic quadrilateral element is employed to model the piezoelectric patch. By imposing the continuity conditions for the displacement and the forces in the interface, the governing equations of the structure can be derived. Reflection coefficients can be obtained by using virtual work or least square method. By adjusting applied voltage at the end of piezoelectric patch, outgoing energy of the reflected waves can be minimized. This phenomenon is the called energy harvesting. Also by setting appropriate voltage in the patch, the vibration at the end of the patch can be absorbed, which is called passive-control. An optimization method is mentioned to obtain relatively high efficiency of energy harvesting. End resonance is also observed in the numerical study.

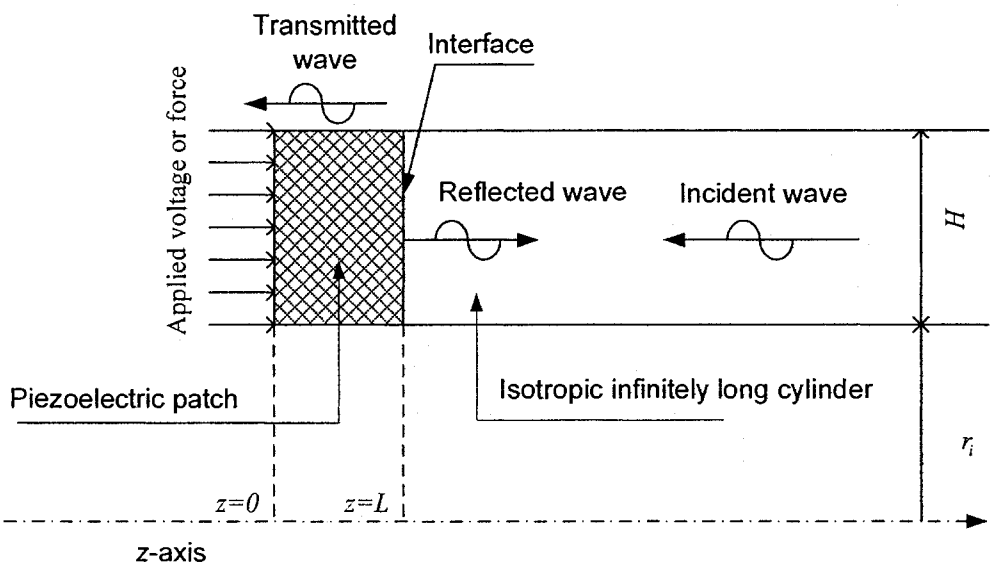

Figure 7. A semi-infinite cylinder with piezoelectric patch

3.2 Model of the piezoelectric patch

Since the geometry, boundary force and material properties of piezoelectric patch are axisymmetric, axisymmetric isoparametric finite-element methodology and numerical integration are used to discretize the patch in the radial and axial directions. The explicit interpolation forms of an eight-node quadratic element shown in Figure 8 in the physical element are given by

$$
\begin{aligned}
&n_1(\xi,\eta)=\frac{1}{4}(1-\xi)(1-\eta)(-\xi-\eta-1), \quad n_2(\xi,\eta)=\frac{1}{4}(1+\xi)(1-\eta)(+\xi-\eta-1),\\
&n_3(\xi,\eta)=\frac{1}{4}(1+\xi)(1+\eta)(+\xi+\eta-1), \quad n_4(\xi,\eta)=\frac{1}{4}(1-\xi)(1+\eta)(-\xi+\eta-1),\\
&n_5(\xi,\eta)=\frac{1}{2}(1-\xi^2)(1-\eta) \quad , \quad n_6(\xi,\eta)=\frac{1}{2}(1-\eta^2)(1+\xi),\\
&n_7(\xi,\eta)=\frac{1}{2}(1-\xi^2)(1+\eta) \quad , \quad n_8(\xi,\eta)=\frac{1}{2}(1-\eta^2)(1-\xi),
\end{aligned}
\tag{3.1}
$$

where ξ and η are local variables in an eight-node isoparametric element $(-1\le\xi\le+1,-1\le\eta\le+1)$.

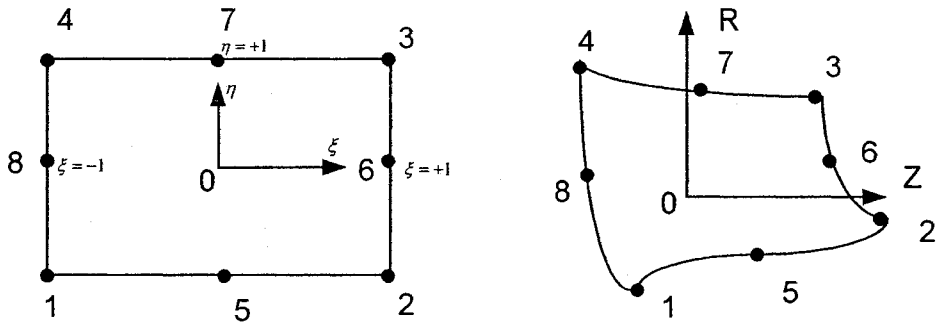

Figure 8. Parent element and slave element

According to the interpolation functions, the interpolations of the geometry and any one of the field variables, say x, over the isoparametric element are given by

$$x = \sum_{i=1}^{8} n_i(\xi,\eta)\, x_i \,. \tag{3.2}$$

The field variables $\{\mathbf{v}_e\}$ in an eight-node quadratic element can be written as

$$\{\mathbf{v}_e(r,\theta,z,t)\} = [N_e(\xi,\eta)]\{\mathbf{V}_e(\theta,t)\}, \tag{3.3}$$

where

$$[N_e(\xi,\eta)] = \begin{bmatrix} n_1 & \cdots & n_8 & & & & & & & & & \\ & & & n_1 & \cdots & n_8 & & & & & & \\ & & & & & & n_1 & \cdots & n_8 & & & \\ & & & & & & & & & n_1 & \cdots & n_8 \end{bmatrix},$$

$$\{\mathbf{V}_e\} = [\mathbf{V}_1 \quad \mathbf{V}_2 \quad \cdots \quad \mathbf{V}_8]^T = [u_{1r} \quad \cdots \quad u_{8r} \quad u_{1\theta} \quad \cdots \quad u_{8\theta} \quad u_{1z} \quad \cdots \quad u_{8z} \quad \phi_1 \quad \cdots \quad \phi_8]^T,$$

and $[N_e(\xi, \eta)]$ is the finite element interpolation matrix and $\{\mathbf{V}_e\}$ denotes the nodal displacement and electric potential in an eight-node quadratic element.

The general strain-displacement relations in the piezoelectric patch can be given by

$$\begin{aligned} \{\mathbf{q}\} &= [\mathbf{L}]\{\mathbf{v}\} = [\mathbf{L}]([N(\xi,\eta)]\{\mathbf{V}\}) \\ &= [\mathbf{L}_r]([N(\xi,\eta)]\{\mathbf{V}\}) + [\mathbf{L}_\theta]([N(\xi,)]\{\mathbf{V}\}) + [\mathbf{L}_z]([N(\xi,\eta)]\{\mathbf{V}\}) \\ &= [\tilde{B}_1]\{\mathbf{V}\} + [\tilde{B}_2]\{\mathbf{V}_{,\theta}\}, \end{aligned} \tag{3.4}$$

where differential operators $[\mathbf{L}_r]$, $[\mathbf{L}_\theta]$, $[\mathbf{L}_z]$ are discussed in Chapter 2 and $[\tilde{B}_1], [\tilde{B}_2]$

are given in Appendix.

By substitution of equation (3.4) into the Hamilton principle, the following equation of motion can be derived

$$\left[\tilde{K}_{11}\right]\{\mathbf{V}\}+\left[\tilde{K}_{12}\right]\{\mathbf{V}_{,\theta}\}-\left[\tilde{K}_{21}\right]\{\mathbf{V}_{,\theta}\}-\left[\tilde{K}_{22}\right]\{\mathbf{V}_{,\theta\theta}\}+\left[\tilde{M}\right]\{\ddot{\mathbf{V}}\}=\{\mathbf{F}\}\ , \qquad (3.5)$$

where

$$\left[\tilde{K}_{11}\right]=\iiint\left[\tilde{B}_1\right]^T\left[\mathbf{C}^{**}\right]\left[\tilde{B}_1\right]rdrdz,\ \ \left[K_{12}\right]=\iiint\left[\tilde{B}_1\right]^T\left[\mathbf{C}^{**}\right]\left[\tilde{B}_2\right]rdrdz,$$
$$\left[\tilde{K}_{21}\right]=\iiint\left[\tilde{B}_2\right]^T\left[\mathbf{C}^{**}\right]\left[\tilde{B}_1\right]rdrdz,\ \ \left[\tilde{K}_{22}\right]=\iiint\left[\tilde{B}_2\right]^T\left[\mathbf{C}^{**}\right]\left[\tilde{B}_2\right]rdrdz,$$
$$\left[\tilde{M}\right]=\iiint\left[N(\xi,\eta)\right]^T[\boldsymbol{\rho}]\left[N(\xi,\eta)\right]rdrdz,$$

and matrices $[\mathbf{C}^{**}]$, $[\rho]$ are given in the previous chapter. Note that integrals in the radial direction have lower and upper limits of inner radius r_i and r_o, and integrals in the axial direction have lower and upper limits of 0 and z_0.

Because of axisymmetric structure, the solutions $\{\mathbf{V}\}$ and $\{\mathbf{F}\}$ for the harmonic motion have the forms of

$$\begin{aligned}\{\mathbf{V}\}&=\{\mathbf{V}_0\}e^{i(m\theta-\omega t)}\\ \{\mathbf{F}\}&=\{\mathbf{F}_0\}e^{i(m\theta-\omega t)}\end{aligned}, \qquad (3.6)$$

where ω is the normalized circular frequency, m is the circumferential wave number, $\{\mathbf{V}_0\}$ the modal distribution of mechanical displacements and electric potential, and $\{\mathbf{F}_0\}$ the modal distribution of force and electric displacement.

Substituting equation (3.6) into equation (3.5) gives rise to

$$\left[\tilde{K}\right]\{\mathbf{V}_0\}=\{\mathbf{F}_0\} \qquad (3.7)$$

where

$$\left[\tilde{K}\right]=\left(\left[\tilde{K}_{11}\right]+mi\left[\tilde{K}_{12}\right]-mi\left[\tilde{K}_{21}\right]+m^2\left[\tilde{K}_{22}\right]-\omega^2\left[\tilde{M}\right]\right)=\begin{bmatrix}[S_{II}] & [S_{IB}]\\ [S_{BI}] & [S_{BB}]\end{bmatrix},$$

$$\{\mathbf{F}_0\}=\begin{Bmatrix}\mathbf{F}_I\\ \tilde{\mathbf{F}}_B\end{Bmatrix},\ \ \{\mathbf{V}_0\}=\begin{Bmatrix}\mathbf{V}_I\\ \tilde{\mathbf{V}}_B\end{Bmatrix},$$

and $\{\mathbf{F}_I\}$ and $\{\tilde{\mathbf{F}}_B\}$ are nodal forces and electric displacements in interior areas of

piezoelectric patch and in the interface, respectively. $\{\mathbf{V}_I\}$ and $\{\tilde{\mathbf{V}}_B\}$ are nodal displacements and electric potential in interior areas of piezoelectric patch and in the interface, respectively.

3.3 Wave function expansion

Propagating and non-propagating waves in a cylinder have been discussed in the previous chapter. For a semi-infinitely long cylinder with piezoelectric patch, the reflected and transmitted waves occur when an incident wave strikes the interface. The reflected waves contain a finite number of propagating waves and an infinite number of non-propagating waves. The semi-analytical finite element method, as discussed in Chapter 2, is employed here to study the reflected wave field in the semi-infinite cylinder.

The nodal displacements and electric potential $\{\mathbf{V}^s\}$ corresponding to the reflected wave field of a semi-infinitely long cylinder can be represented by

$$\{\mathbf{V}^s\} = \sum_{j=1}^{M} D_j \{\mathbf{V}_j\}, \tag{3.8}$$

where

$$D_j = R_j e^{ik_m L}$$
$$\{\mathbf{V}_j\} = \{\mathbf{V}_{1j} \quad \mathbf{V}_{2j} \quad \cdots \quad \mathbf{V}_{kj} \quad \cdots \quad \mathbf{V}_{NPj}\}^T,$$
$$\{\mathbf{V}_{kj}\} = \{u_{rkj} \quad u_{\theta kj} \quad u_{zkj} \quad \phi_{kj}\}^T$$

and $\{\mathbf{V}_j\}$ is the jth wave mode corresponding to the wave number k_m, NP is the number of nodes in the radial direction, L is the thickness of the patch, and R_j is the unknown reflection coefficient of the jth wave mode.

The compact form of equation (3.8) is given as

$$\{\mathbf{V}^s\} = [\mathbf{G}]\{\mathbf{D}\}, \tag{3.9}$$

where

$$[\mathbf{G}] = [\mathbf{V}_1 \quad \mathbf{V}_2 \quad \cdots \quad \mathbf{V}_M],$$
$$\{\mathbf{D}\} = \{D_1 \quad D_2 \quad \cdots \quad D_M\}.$$

The equivalent force and electric displacement of the reflected wave can be obtained from the wave mode by using general stress-strain and strain-displacement relations given in Chapter 2, and they can be written as follows

$$\{\mathbf{F}^s\} = \sum_{j=0}^{M} R_j \{\mathbf{F}_j\} e^{ik_m L}, \tag{3.10}$$

where

$$\{\mathbf{F}_j\} = \{\mathbf{F}_{1j} \quad \mathbf{F}_{2j} \quad \ldots \quad \mathbf{F}_{kj} \quad \ldots \quad \mathbf{F}_{NPj}\}^T$$
$$\{\mathbf{F}_{kj}\} = \{\mathbf{f}_{rkj} \quad \mathbf{f}_{\theta kj} \quad \mathbf{f}_{zkj} \quad \mathbf{d}_{zkj}\}^T.$$

$\{\mathbf{F}_j\}$ is the jth wave mode containing forces and electric displacement corresponding to the wave number k_j.

The compact form of equation (3.10) has the expression

$$\{\mathbf{F}^s\} = [\mathbf{F}]\{\mathbf{D}\}, \tag{3.11}$$

where $[\mathbf{F}] = [\mathbf{F}_1 \; \mathbf{F}_2 \ldots \mathbf{F}_M]$.

The nodal displacements and electric potential, $\{\mathbf{V}_B^{in}\}$,and the nodal equivalent force and electric displacement, $\{\mathbf{F}_B^{in}\}$, corresponding to the incident wave traveling from negative z-axis to origin can be written as

$$\{\mathbf{V}_B^{in}\} = R_{in}\{\mathbf{V}_{in}\} e^{ik_m L},$$
$$\{\mathbf{F}_B^{in}\} = R_{in}\{\mathbf{F}_{in}\} e^{ik_m L}. \tag{3.12}$$

The total wave field in the cylinder is then given by a summation of the incident wave and reflected wave. As a result, the nodal displacements, forces, electric potential and electric displacement at the interface between the cylinder and the patch are then given by

$$\begin{aligned} \{\mathbf{V}_B\} &= \{\mathbf{V}_B^s\} + \{\mathbf{V}_B^{in}\} \\ \{\mathbf{F}_B\} &= \{\mathbf{F}_B^s\} + \{\mathbf{F}_B^{in}\} \end{aligned}, \tag{3.13}$$

where

$$\begin{aligned} \{\mathbf{V}_B^s\} &= [G]\{\mathbf{D}\}, \\ \{\mathbf{F}_B^s\} &= [F]\{\mathbf{D}\}, \end{aligned}$$

here $\{\mathbf{V}_B^s\}$ are the nodal displacements and electric potentials of the reflected waves in interface, and $\{\mathbf{F}_B^s\}$ are the nodal forces and electric displacements of the reflected waves in interface.

3.4 Hybrid method

Using the virtual work principle, equation (3.7) can be written as

$$\{\delta\bar{\mathbf{V}}_I^T \quad \delta\bar{\tilde{\mathbf{V}}}_B^T\}\begin{bmatrix} S_{II} & S_{IB} \\ S_{BI} & S_{BB} \end{bmatrix}\begin{Bmatrix} \mathbf{V}_I \\ \tilde{\mathbf{V}}_B \end{Bmatrix} = \{\delta\bar{\mathbf{V}}_I^T \quad \delta\bar{\tilde{\mathbf{V}}}_B^T\}\begin{Bmatrix} \mathbf{F}_I \\ \tilde{\mathbf{F}}_B \end{Bmatrix}, \tag{3.14}$$

where δ represents the first variation and over bar denotes complex conjugate. Here $\{\tilde{\mathbf{V}}_B\}$ is the nodal displacements and electric potentials of the piezoelectric patch at the interface, $\{\tilde{\mathbf{F}}_B\}$ the equivalent nodal forces and electric displacements applying to piezoelectric patch through the interface, $\{\mathbf{V}_B\}$ the nodal displacements and electric potentials of the semi-infinitely long cylinder at interface; and $\{\mathbf{F}_B\}$ the equivalent nodal forces and electric displacements applying to the semi-infinitely long cylinder through the interface.

The above equation can be written as

$$[S_{II}]\{\mathbf{V}_I\}+[S_{BI}]\{\mathbf{V}_I\}=\{\mathbf{F}_I\},$$
$$\delta\left\{\bar{\tilde{\mathbf{V}}}_B\right\}^T[S_{IB}]\{\tilde{\mathbf{V}}_B\}+\delta\left\{\bar{\tilde{\mathbf{V}}}_B\right\}^T S_{BB}\{\tilde{\mathbf{V}}_B\}=\delta\left\{\bar{\tilde{\mathbf{V}}}_B\right\}^T\{\tilde{\mathbf{F}}_B\}. \tag{3.15}$$

The nodal displacement and electric potential in the interior area can be represented by

$$\{\mathbf{V}_I\}=[S_{II}]^{-1}\left(\{\mathbf{F}_I\}-[S_{IB}]\{\tilde{\mathbf{V}}_B\}\right). \tag{3.16}$$

Substitution of equation (3.16) into equation (3.7), it's found that $\{\tilde{\mathbf{V}}_B\}$ must satisfy

$$\delta\left\{\bar{\tilde{\mathbf{V}}}_B\right\}^T\left[S^*_{BB}\right]\{\tilde{\mathbf{V}}_B\}=\delta\left\{\bar{\tilde{\mathbf{V}}}_B\right\}^T\left(\{\tilde{\mathbf{F}}_B\}-[S_{BI}][S_{II}]^{-1}\{\mathbf{F}_I\}\right), \tag{3.17}$$

where $\left[S^*_{BB}\right]=[S_{BB}]-[S_{BI}][S_{II}]^{-1}[S_{IB}]$.

By imposing continuity condition for the displacements, electric potential, forces and electric displacement at interface of piezoelectric patch and the semi-infinitely long cylinder, following equation can be given by

$$\begin{aligned}\{\tilde{\mathbf{V}}_B\}&=\{\mathbf{V}_B\},\\ \{\tilde{\mathbf{F}}_B\}&=-\{\mathbf{F}_B\},\end{aligned} \tag{3.18}$$

Substituting equation (3.18) into equation (3.17) yields

$$\begin{aligned}&\delta\{\bar{\mathbf{V}}\}_B^T=\delta\{\bar{\mathbf{D}}\}^T[G]^T,\\ &\delta\{\bar{\mathbf{D}}\}^T\left(\left[\bar{G}\right]^T\left(\left[S^*_{BB}\right][G]+[F]\right)\{\mathbf{D}\}\right)=\delta\{\bar{\mathbf{D}}\}^T\left(\left[\bar{G}\right]^T\left(-\{\mathbf{F}^{in}_B\}-\left[S^*_{BB}\right]\{\mathbf{V}^{in}_B\}-[S_{BI}][S_{II}]^{-1}\{\mathbf{F}_I\}\right)\right).\end{aligned} \tag{3.19}$$

The virtual work solution of $\{\mathbf{D}\}$ is given as

$$\left[\bar{\mathbf{G}}\right]^T\left(\left[S^*_{BB}\right][G]+[F]\right)\{\mathbf{D}\}=\left[\bar{G}\right]^T\left(-\{\mathbf{F}^{in}_B\}-\left[S^*_{BB}\right]\{\mathbf{q}^{in}_B\}-[S_{BI}][S_{II}]^{-1}\{\mathbf{F}_I\}\right). \tag{3.20}$$

The least-square solution of $\{\mathbf{D}\}$ is given as

$$\overline{\left(\left[S^*_{BB}\right][G]+[F]\right)}^T\left(\left[S^*_{BB}\right][G]+[F]\right)\{\mathbf{D}\}=\overline{\left(\left[S^*_{BB}\right][G]+[F]\right)}^T\left(-\{\mathbf{F}^{in}_B\}-\left[S^*_{BB}\right]\{\mathbf{V}^{in}_B\}-[S_{BI}][S_{II}]^{-1}\{\mathbf{F}_I\}\right). \tag{3.21}$$

3.5 Energy balance

Since only propagating waves carry energy, the outgoing energy is shared by all the participating reflected propagating waves,

$$E_{out} = \sum_{n=1}^{N_{pr}} E_n , \tag{3.22}$$

here E_n is the energy carried by the nth propagating mode, and N_{pr} is the number of propagating modes.

The distribution of energy carried by the nth reflected propagating wave can be expressed by E_n/E_{in}. The energy balance Δ defined as following form is used to check measurement accuracy of solution

$$\Delta = \left[1 - \sum_{n=1}^{N_{pr}} \frac{E_n}{E_{in}} \right] \times 100 . \tag{3.23}$$

3.6 Energy harvest

In this section, three issues are studied: passive end reflection, oscillating voltage applied at the end of the piezoelectric patch, and energy harvesting.

3.6.1 Passive end reflection

Considering the passive reflection of an incoming harmonic wave traveling in the negative z-direction. When the incident wave strikes on the interface between the piezoelectric patch and the cylinder, a reflected wave field is generated.

The mechanical and electric boundary conditions at the end of piezoelectric patch are

$$T_{zz} = T_{z\theta} = T_{zr} = 0, \quad \phi = 0 \quad \text{or} \quad D_z = 0, \quad z = 0. \tag{3.24}$$

Reflection coefficients $\{\mathbf{R}_1\}$ can be calculated by solving equations (3.20) or (3.21) for a given incident wave.

Outgoing energy carried by the reflected propagating waves is given as

$$E_{out} = \left(a^{in}\right)^2 \chi_2, \tag{3.25}$$

where

$$\chi_2 = \sum_{n=1}^{N_{pr}} \bar{g}_n^{in} g_n^{in} J_n,$$

$$\left\{\mathbf{g}^{in}\right\} = \left\{g_1^{in} \quad g_2^{in} \quad \cdots \quad g_{pr}^{in}\right\}^T = \left[\left\langle [F]\ [F] \right\rangle\right]^{-1} \left\langle [F], \left\{\mathbf{Q}^{in}\right\} \right\rangle,$$

and $[F]$ is modal matrix that is given in equation (2.23) and $\{\mathbf{Q}^{in}\}$ is defined in equation (2.21) as distributions of forces and electric displacements stimulated by the given incident wave.

3.6.2 Oscillating end voltage-forced vibration

An oscillating voltage applied at the end of piezoelectric patch will generate time harmonic outgoing waves in a semi-infinitely long cylinder. The boundary condition in the end of piezoelectric patch can be represented as

$$T_{zz} = T_{z\theta} = T_{zr} = 0, \quad \phi(r,t) = \phi_0 v(r) e^{-i\omega t}, \quad z = 0, \tag{3.26}$$

Where: ϕ_0 is the normalized magnitude of applied voltage; ω is the normal circular frequency of oscillating end voltage; and $v(r)$ is the distribution of applied voltage.

The reflection coefficients $\{\mathbf{R}_2\}$ can be calculated by using a similar process as studied in the passive end reflection.

Outgoing energy carried by reflected propagating waves is given as

$$E_{out} = \phi_0^2 \chi_0, \tag{3.27}$$

where

$$\chi_0 = \sum_{n=1}^{N_{pr}} \bar{g}_n^{\phi} g_n^{\phi} J_n,$$

$$\left\{\mathbf{g}^{\phi}\right\} = \left\{g_1^{\phi} \quad g_2^{\phi} \quad \cdots \quad g_{pr}^{\phi}\right\}^T = \left[\left\langle [F]\ [F] \right\rangle\right]^{-1} \left\langle [F], \left\{\mathbf{Q}^{\phi}\right\} \right\rangle,$$

and $\{\mathbf{Q}^{\phi}\}$ is defined in equation (2.21) as the distributions of forces and electric displacements stimulated by oscillating end voltage.

3.6.3 Semi-active end reflection

Consider the presence of an incoming monochromatic wave whose reflection occurs with an oscillating end voltage. The mechanical and electric boundary conditions at $z = 0$ in piezoelectric patch are

$$T_{zz} = T_{z\theta} = T_{zr} = 0, \quad \phi(r,t) = \phi_0 v(r) e^{-i\omega t}, \quad z = 0 \tag{3.28}$$

Since both passive end reflection and vibration generated by oscillating end voltage are linear systems, reflection coefficients $\{\mathbf{R}_3\}$ are the sum of reflection coefficients $\{\mathbf{R}_1\}$ and $\{\mathbf{R}_2\}$, i.e.,

$$\left\{\mathbf{R}_3\right\} = \left\{\mathbf{R}_1\right\} + \left\{\mathbf{R}_2\right\} \tag{3.29}$$

The outgoing energy is given by

$$E_{out} = \left(a^{in}\right)^2 \chi_2 - a^{in}\phi_0 \chi_1 + \phi_0^2 \chi_0, \tag{3.30}$$

where

$$\chi_1 = \sum_{n=1}^{N_{pr}} \left(\bar{g}_n^{\phi} g_n^{in} + g_n^{\phi} \bar{g}_n^{in}\right) J_n.$$

3.6.4 Minimizing outgoing energy

For Action 3.6.3, it can be seen that the outgoing energy carried by each propagating mode is strongly depended on the applied end voltage. Thus, the total outgoing energy can be minimized by carefully selecting the end voltage, ϕ_0. This method is called as passive vibration control.

The second derivative of E_{out} in equation (3.30) is found positive. This is because

$$\frac{d^2 E_{out}}{d\phi_0^2} = 2\chi_0, \tag{3.31}$$

and χ_0 is positive. The minimal outgoing energy can then be found by setting the first derivative of E_{out} is zero.

By differentiating the equation (3.30), the minimal of E_{out} can be written as

$$\frac{dE_{out}}{d\phi_0} = 2\phi_0\chi_0 - a^{in}\chi_1 = 0 \rightarrow \phi_0 = \frac{\chi_1}{2\chi_0}a^{in}, \tag{3.32}$$

Therefore, the minimized outgoing energy flux of the reflected wave is

$$E_{out} = \left(a^{in}\right)^2\left[\chi_2 - \frac{\chi_1^2}{4\chi_0}\right]. \tag{3.33}$$

3.7 Numerical study

3.7.1 Verification of the computer code

A FORTRAN computer code was developed in the study. First, convergence of the numerical procedure is tested with different mesh sizes, and results are compared with published data. For each case, a different number of axial modes is chosen in the wave function expansion to ensure convergence of the numerical procedure. The need meshes are listed in Table 2. Table 3 was the rate of convergence of the mesh sizes for the reflection coefficients.

As noted in the previous section, the accuracy of the numerical procedure was tested by calculating the energy balance:

$$\Delta = \frac{E_{input} - E_{out}}{E_{input}} \times 100\% . \tag{3.34}$$

In the numerical case studied herein, energy balance coefficient Δ is less than 0.001%.

The test problem considered was investigated by Bai *et al.* [28]. They used the one dimensional finite element method to analyze the problem. The geometry of the cylinder is given by H/R = 1, H = 1, normalized thickness of the end area (L = 0.1), and circumferential wave number is m = 0. The piezoelectric material constants are given by

$$[\tilde{\mathbf{C}}] = 10^{10}\begin{bmatrix} 13.90 & 7.78 & 7.43 & . & . & . \\ . & 13.90 & 7.43 & . & . & . \\ . & . & 13.90 & . & . & . \\ . & . & . & 2.56 & . & . \\ . & \text{symmetric} & . & . & 2.56 & . \\ . & . & . & . & . & 3.06 \end{bmatrix} \text{Pa},$$

$$[\tilde{\mathbf{e}}] = \begin{bmatrix} . & . & . & . & 12.70 & . \\ . & . & . & 12.70 & . & . \\ -5.20 & -5.20 & 15.10 & . & . & . \end{bmatrix} \text{C/m}^2,$$

$$[\tilde{\boldsymbol{\varepsilon}}] = 10^{-7}\begin{bmatrix} .1306 & . & . \\ . & .1306 & . \\ . & . & .1151 \end{bmatrix} \text{F/m}.$$

The normalized properties of piezoelectric material are

$$[\mathbf{C}] = \begin{bmatrix} 5.42969 & 3.03906 & 2.90234 & . & . & . \\ . & 5.42969 & 2.90234 & . & . & . \\ . & . & 4.49219 & . & . & . \\ . & . & . & 1.0 & . & . \\ . & \text{symmetric} & . & . & 1.0 & . \\ . & . & . & . & . & 1.19531 \end{bmatrix},$$

$$[\mathbf{e}] = \begin{bmatrix} . & . & . & . & 0.84106 & . \\ . & . & . & 0.84106 & . & . \\ -0.34437 & -0.34437 & 1.0 & . & . & . \end{bmatrix},$$

$$[\boldsymbol{\varepsilon}] = \begin{bmatrix} 1.46632 & . & . \\ . & 1.46632 & . \\ . & . & 1.29229 \end{bmatrix}$$

Table 2. Six different mesh sizes

Size	Size 1	Size 2	Size 3	Size 4	Size 5	Size 6
N_r	10	20	40	10	20	40
N_z	1	1	1	2	2	2

N_r is the number of elements in the radial direction, N_z is the number of element in the axial direction.

Table 3. Convergence check for different mesh sizes

Ref coe / Mesh type	$\|R_1\|$	$\|R_2\|$	$\|R_3\|$
2D 10_1	0.03273647	0.08433736	1.18967382
2D 20_1	0.03271132	0.08462933	1.18155558
2D 40_1	0.03270966	0.08477917	1.17717375
2D 10_2	0.03271864	0.08433484	1.18967474
2D 20_2	0.03269511	0.08462702	1.18155644
2D 40_2	0.03269356	0.08477691	1.17717452
Published result	0.03269237	0.08477675	1.17717459

End reflection is examined first. Table 3 shows the first three reflection coefficients of propagating waves (R_1, R_2 and R_3). Here the incident wave is the first longitudinal wave mode and the normalized circular frequency is $\omega = 5.0$. It can be seen from Table 3 that the results from the current method converged to the semi-analytical results (the last row of Table 3). By comparing the amplitudes of reflection coefficients of different mesh, it can be seen that the mesh $N_z = 20$, $N_r = 1$ is sufficient in the computation. The relative error between the current method and the 1-D model (the model used in [28]) is less than 0.4%.

Next, the motion of the cylinder due to an applied end voltage as well as an incident wave is studied. The normalized frequency of the applied end voltage is checked in a narrow 'backward wave' range ($2.205 < \omega < 2.221$).

Shown in Figure 9 and Figure **10** is the amplitude and energy carried by each propagating mode derived from the current method and [28]. Type 1 is published 1-D model and type 2 is our developed model. The results from the two methods are in very good agreement. It may be worth mentioning that there is a backward wave in the frequency range [28].

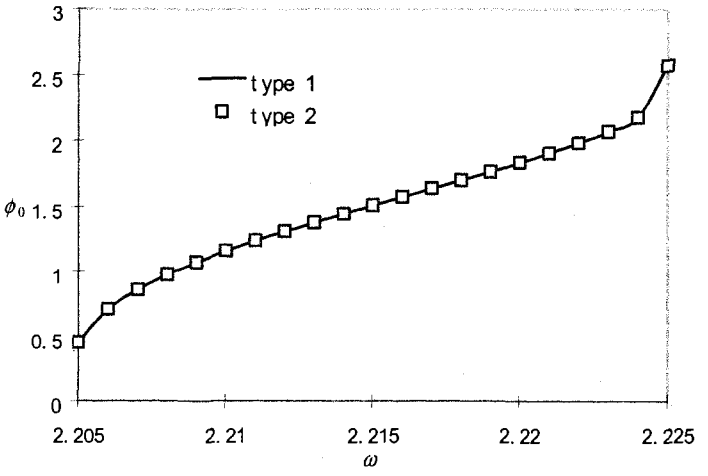

Figure 9. Amplitudes of applied voltage

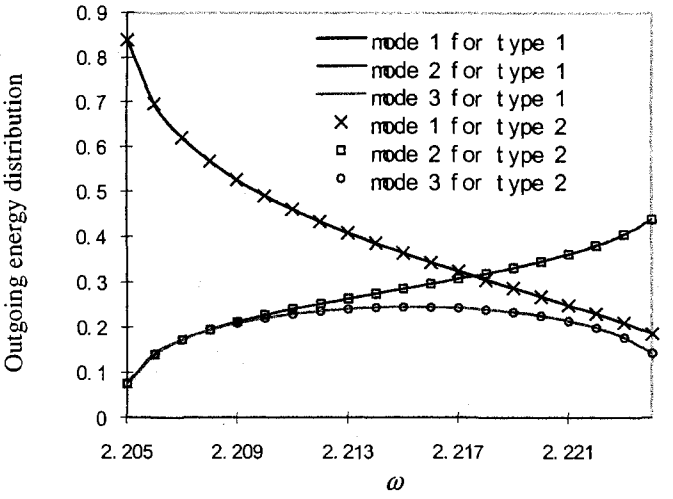

Figure 10. Energy distribution of reflected waves

3.7.2 Numerical studies

This subsection presents numerical results from investigating energy harvest and end resonance in a semi-infinite isotropic cylinder with attached piezoelectric patch.

Two cylinders are studied here. One is a thick cylinder having H/R = 1 and the other a thin cylinder having H/R = 0.135, where H is the thickness and R is the mean

radius of the cylinder. In each cylinder, two different circumferential wave numbers, m, are considered, i.e., $m = 0$ and $m = 1$. Different boundary conditions ($D_z = 0$ or $\phi = 0$) of the electric filed at the interface are considered. The variations of the thickness (L = 0.025, 0.05, 0.75 and 0.1) of the patch and the distribution of applied end voltage are also studied.

The normalization constants are: (1) elastic modulus $c^0 = 0.8427\times10^{11}$ Pa, (2) piezoelectric constant $\varepsilon^0 = 0.1151\times10^{-7}$ F/m, and (3) mass density $\rho^0 = 7.8\times10^3$ kg/m^3.

The material constants of steel are given by

$$[\tilde{\mathbf{C}}] = 10^{11}\begin{bmatrix} 2.8207 & 1.1354 & 1.1354 & . & . & . \\ 1.1354 & 2.8207 & 1.1354 & . & . & . \\ 1.1354 & 1.1354 & 2.8207 & . & . & . \\ . & . & . & 0.8427 & . & . \\ . & . & . & . & 0.8427 & . \\ . & . & . & . & . & 0.8427 \end{bmatrix}_{6\times6} \text{Pa.}$$

The normalized material constants of steel are given by

$$[\mathbf{C}] = \begin{bmatrix} 3.3474 & 1.34742 & 1.34742 & . & . & . \\ 1.34742 & 3.3474 & 1.34742 & . & . & . \\ 1.34742 & 1.34742 & 3.3474 & . & . & . \\ . & . & . & 1 & . & . \\ . & . & . & . & 1 & . \\ . & . & . & . & . & 1 \end{bmatrix}_{6\times6}$$

The material constants of the piezoelectric patch are given by

$$[\mathbf{C}] = 10^{10}\begin{bmatrix} 13.90 & 7.78 & 7.43 & . & . & . \\ . & 13.90 & 7.43 & . & . & . \\ . & . & 13.90 & . & . & . \\ . & . & . & 2.56 & . & . \\ . & \text{symmetric} & . & . & 2.56 & . \\ . & . & . & . & . & 3.06 \end{bmatrix} \text{Pa,}$$

$$[\mathbf{e}] = \begin{bmatrix} . & . & . & . & 12.70 & . \\ . & . & . & 12.70 & . & . \\ -5.20 & -5.20 & 15.10 & . & . & . \end{bmatrix} \text{C/m}^2\text{,}$$

$$[\varepsilon]=10^{-7}\begin{bmatrix}0.13060 & . & . \\ . & 0.13060 & . \\ . & . & 0.115102\end{bmatrix}\text{F/m.}$$

The normalized material properties of the piezoelectric patch are shown in below

$$[\mathbf{C}]=\begin{bmatrix}1.6495 & 0.92327 & 0.881735 & . & . & . \\ 0.92327 & 1.6495 & 2.90234 & . & . & . \\ 0.881735 & 2.90234 & 1.36473 & . & . & . \\ . & . & . & 0.303801 & . & . \\ . & . & . & . & 0.303801 & . \\ . & . & . & . & . & 0.363137\end{bmatrix},$$

$$[\mathbf{e}]=\begin{bmatrix}. & . & . & . & 0.40779 & . \\ . & . & . & 0.40779 & . & . \\ -0.166969 & -0.166969 & 0.484853 & . & . & .\end{bmatrix},$$

$$[\varepsilon]=\begin{bmatrix}0.113462 & . & . \\ . & 0.113462 & . \\ . & . & 1\end{bmatrix}.$$

Results of different thickness of piezoelectric patches are given to study the effect of piezoelectric patches on the energy harvesting and end resonance. At the same time, three distributions of applied voltage at the end of the piezoelectric patch are presented to study their influence on energy harvesting and end resonance.

3.7.2.1 Energy harvest

Thick cylinder with piezoelectric patch for $m = 0$

Case 1(A). End reflection and energy distribution for L = 0.1

In case 1 (A), energy distribution due to an incident wave is investigated. The incident wave is taken as the first axisymmetric wave. The electric boundary conditions at the end of piezoelectric patch ($z = 0$) and the interface ($z = z_0$) are open circuits ($D_z = 0$).

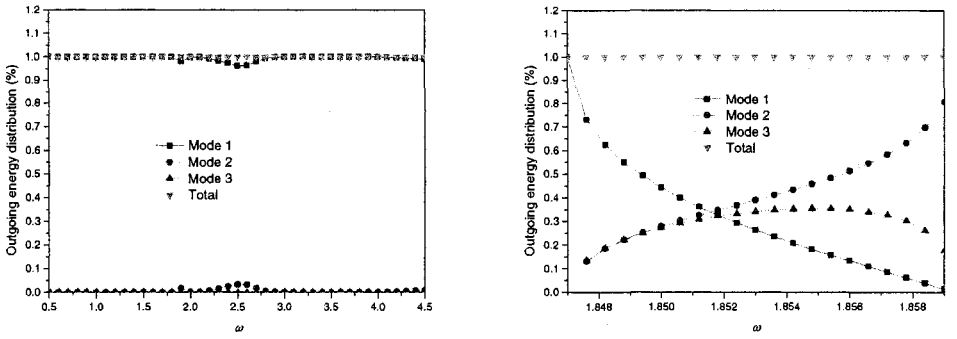

Figure 11. Energy distributions for $m = 0$

As shown in Figure 11(a), it can be seen that the first mode is the dominant mode in the frequency range of interested $0.5 < \omega < 4.5$. In the frequency range of interested $1.847 < \omega < 1.859$, there is a 'backward wave' discussed in the previous chapter. Outgoing energy distribution of the 'backward wave' is plotted in Figure 11(b). There is one propagating wave when $0.5 < \omega < 1.847$; three propagating waves exist when $1.847 < \omega < 1.859$ because of backward wave; when $1.859 < \omega < 3.271$, two propagating waves exist.

Case 1(B). End reflection and energy harvest for L = 0.1 with applied voltage

In case 1(B), In Energy harvest is studied by applying appropriate voltage at the end of the piezoelectric patch. The applied voltage distribution is given by

$$v(r) = \begin{cases} -1 & 0.5 \le r \le 1.0 \\ 1 & 1.0 \le r \le 1.5 \end{cases}. \tag{3.35}$$

Other conditions are same as case 1(A).

Different electric boundary conditions at the interface, namely open circuit $D_z = 0$ and grounded $\phi = 0$, are studied.

Figures 12(a) and (b) show the reflection coefficients of the open and grounded circuit boundary conditions, respectively. On the other hand, the energy distributions carried by the outgoing wave for the two boundary conditions are shown in Figure 13.

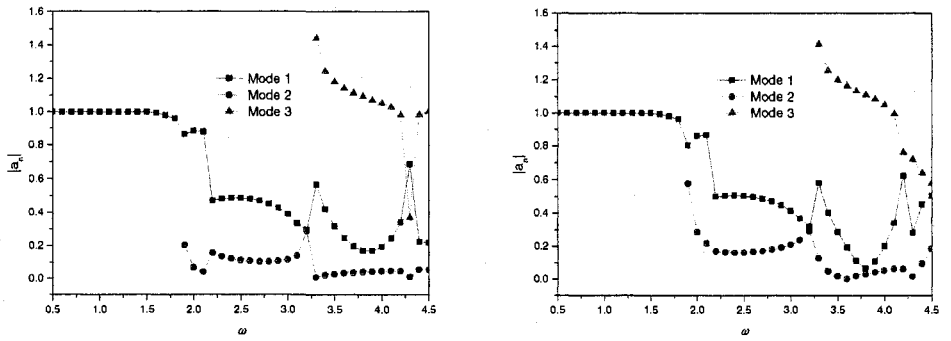

(a) Open circuit (b) Grounded circuit

Figure 12. Reflection coefficients for $m = 0$

As shown in Figure 13(a), when normalized circular frequency of interested $0.5 < \omega < 1.847$ only one propagating wave carries the outgoing energy. The outgoing energy of reflection waves is equal to the incoming energy of the incident wave at $0.5 < \omega < 1.5$. When normalized circular frequency ω is 1.8, the outgoing energy slightly decreases to 92.54%.

In the frequency range of interested $1.847 < \omega < 1.859$, energy distribution of the 'backward wave' is investigated. Figures 13(c) and (d) show the energy carried by reflected waves for the open and grounded circuit boundary conditions, respectively. The outgoing energy decreases a little for open and grounded circuit boundary conditions comparing with that for no applied voltage condition.

Relatively, low and almost constant outgoing energy occurs during the frequency range of interested $2.2 < \omega < 3.2$. The minimal outgoing energy is 14.59% at $\omega = 2.9$. Two propagating reflected waves share the whole outgoing energy. Major part of the outgoing energy is carried by the first propagating wave. When $3.0 < \omega < 4.5$, three propagating waves share the outgoing energy. Low outgoing energy takes place in a narrow range around $\omega = 3.2$ and outgoing energy is 59.75%. In this frequency range, the third propagating mode is the dominant mode.

In the Figure 13(b), the behavior of the outgoing energy for the grounded circuit condition is similar to that of the open circuit. At $\omega = 1.9$, the second propagating

wave shares 25.78% which is higher than that in the open circuit, a merely 3.21%. At $\omega = 4.5$, three propagating waves share 25.57%, 3.48% and 31.35% comparing with those of 4.63%, 0.29% and 93.82% in the open circuit case.

However, the amplitudes of applied voltage, ϕ_0, for the grounded and open circuit are totally different. Detailed discussion will be given in the following case.

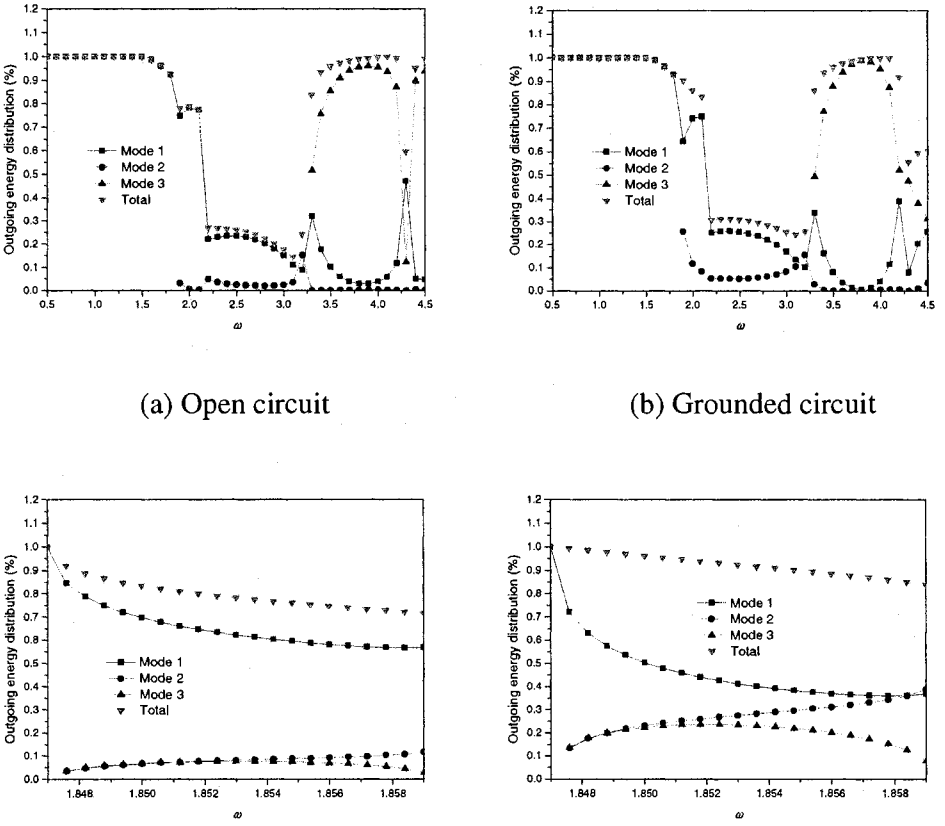

(a) Open circuit (b) Grounded circuit

(c) Open circuit in $1.847 < \omega < 1.859$ (d) Grounded circuit in $1.847 < \omega < 1.859$

Figure 13. Energy distribution for $m = 0$

Case 2. Effects of the thickness of the patch on the energy harvest

Four different normalized thicknesses of the patch, namely L = 0.025, 0.05, 0.075, 0.1, are used to study their effects on energy harvest. The other conditions are the same as those in Case 1.

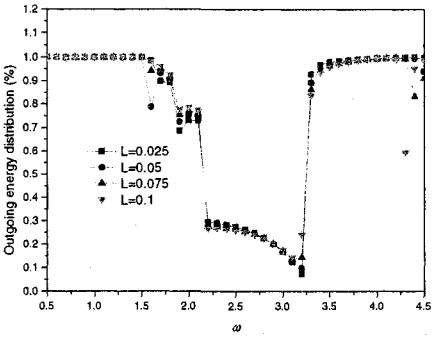

(a) Open circuit

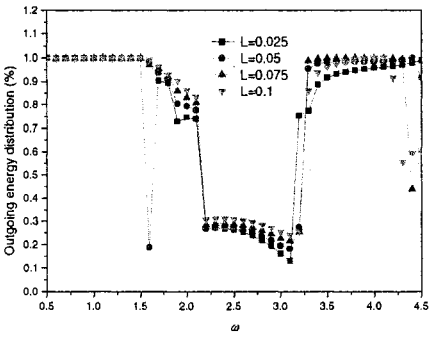

(b) Grounded circuit

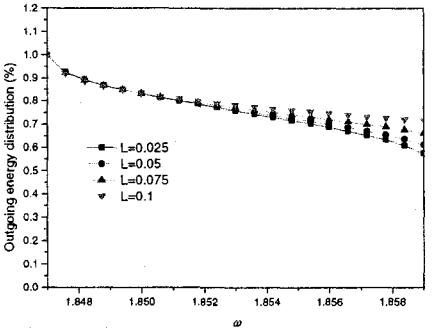

(c) Open circuit in $1.847 < \omega < 1.859$

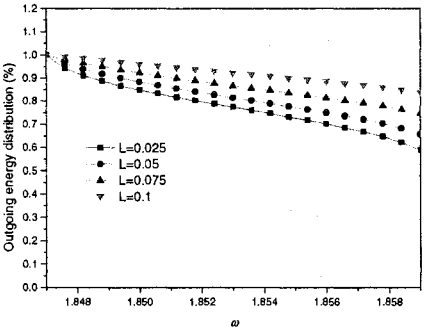

(d) Grounded circuit in $1.847 < \omega < 1.859$

Figure 14. Outgoing energy for different thickness of the patch

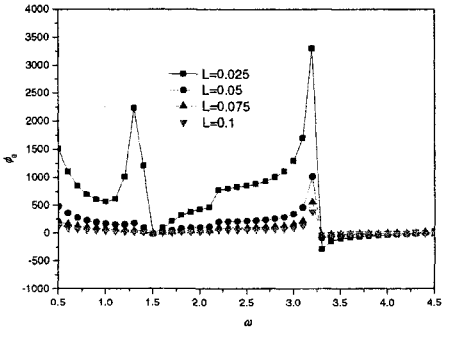

(a) Open circuit

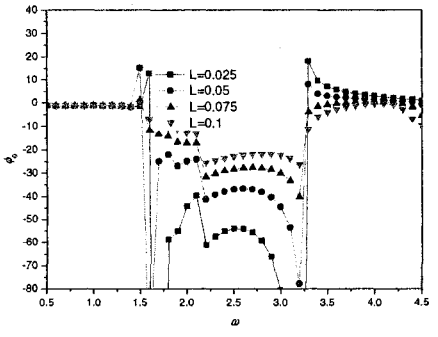

(b) Grounded circuit

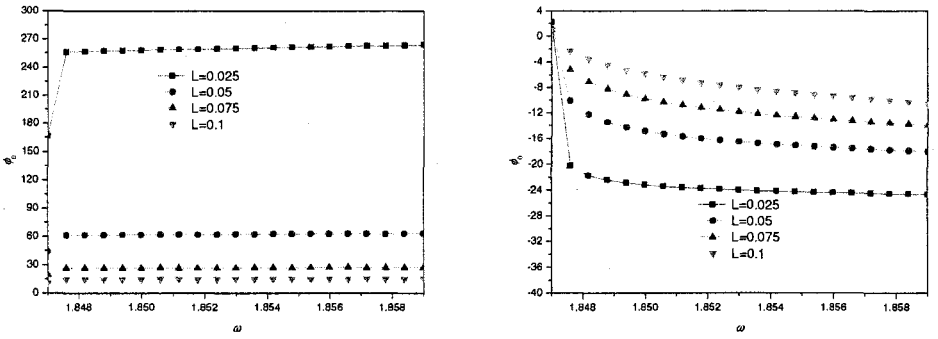

(c) Open circuit in $1.847 < \omega < 1.859$ (d) Grounded circuit in $1.847 < \omega < 1.859$

Figure 15. Magnitudes of applied voltage for different thickness of the patch

When normalized thickness of the piezoelectric patch varies from 0.025 to 0.1, energy distribution of reflected waves and magnitude of applied voltage are shown in Figure 14 and Figure **15**. In Figure 15, the difference of the minimized outgoing energy between the open and grounded circuit conditions is very limit except in the range of $4.3 < \omega < 4.5$. The energy shared by the propagating modes in the frequency range of $4.3 < \omega < 4.5$ is listed in Table 4 for illustrative purpose. It is also shown that the minimized outgoing energy is less sensitive to the thickness of the patch in the open circuit condition than that in the grounded circuit condition.

Table 4. Outgoing energy for $m = 0$ and grounded circuit condition

ω \ δ	L=0.025	L=0.05	L=0.075	L=0.1
4.3	0.97311	0.99206	0.99439	0.55613
4.4	0.97981	0.99892	0.44022	0.59568
4.5	0.98972	0.91663	0.6065	0.60397

However, as shown in Figure 14(a) and (b), the applied voltage is sensitive to the thickness of the piezoelectric patch. Amplitude of the applied voltage in the thicker piezoelectric patch is much smaller than that in the thinner one. Furthermore, the

magnitude of the applied voltage in open circuit condition is hundreds times larger than that in the grounded circuit condition.

Case 3. Effects of the applied voltage on the energy harvest

In this case, the effects of three different distributions of the applied voltage are investigated. The three distributions are given by

$$v_1(r)=\begin{cases}-1 & 0.5\le r\le 1.0\\ 0.5 & 1.0\le r\le 1.5\end{cases}\quad v_2(r)=\begin{cases}-1 & 0.5\le r\le 1.0\\ 1 & 1.0\le r\le 1.5\end{cases}\quad v_3(r)=\begin{cases}-0.5 & 0.5\le r\le 1.0\\ 1 & 1.0\le r\le 1.5\end{cases}. \quad (3.36)$$

The other conditions are the same as those in case 1.

As shown in Figure 16(a) and Figure **17**(a), in the open circuit condition, outgoing energies of the three voltage distributions are essentially the same when $0 < \omega < 4.5$. The magnitudes of $v_2(r)$ and $v_3(r)$ are similar and the magnitude of $v_1(r)$ is slightly smaller than the magnitudes of $v_2(r)$ and $v_3(r)$ when $0 < \omega < 4.5$.

As shown in Figure 16(b) and Figure **17**(b), in the grounded circuit condition, outgoing energies of $v_1(r)$ and $v_2(r)$ are similar at the frequency range of $0 < \omega < 4.5$ except a little differences at $\omega = 2.2$ and 3.2.

The magnitude and outgoing energy of $v_3(r)$ are totally different from those of $v_1(r)$ and $v_2(r)$ at $2.2 < \omega < 4.5$. In the range of $2.2 < \omega < 2.7$, the outgoing energy of $v_3(r)$ is higher than those of $v_1(r)$ and $v_2(r)$. In the range of $2.8 < \omega < 4.5$, the outgoing energy proportion of $v_3(r)$ is lower than those of $v_1(r)$ and $v_2(r)$. On the other hand, the magnitude of $v_3(r)$ is obviously larger than those of $v_1(r)$ and $v_2(r)$ in the range of $2.2 < \omega < 4.5$.

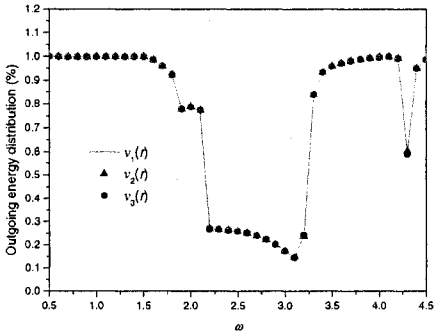

(a) Open circuit

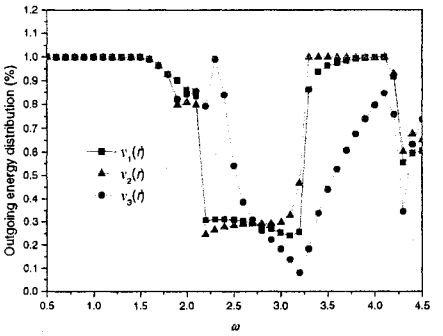

(b) Grounded circuit

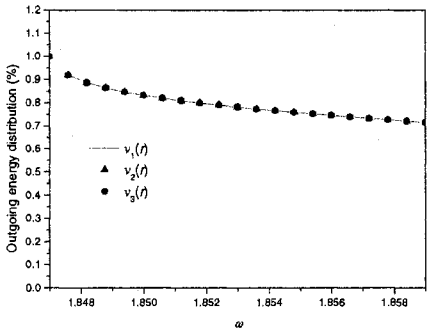

(c) Open circuit in $1.847 < \omega < 1.859$

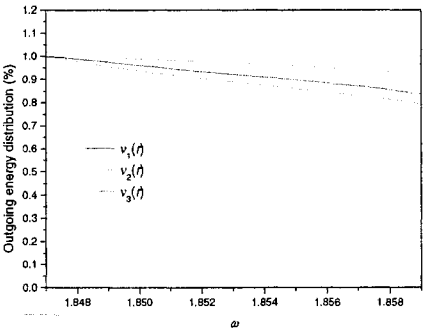

(d) Grounded circuit in $1.847 < \omega < 1.859$

Figure 16. Outgoing energy for different voltage distributions

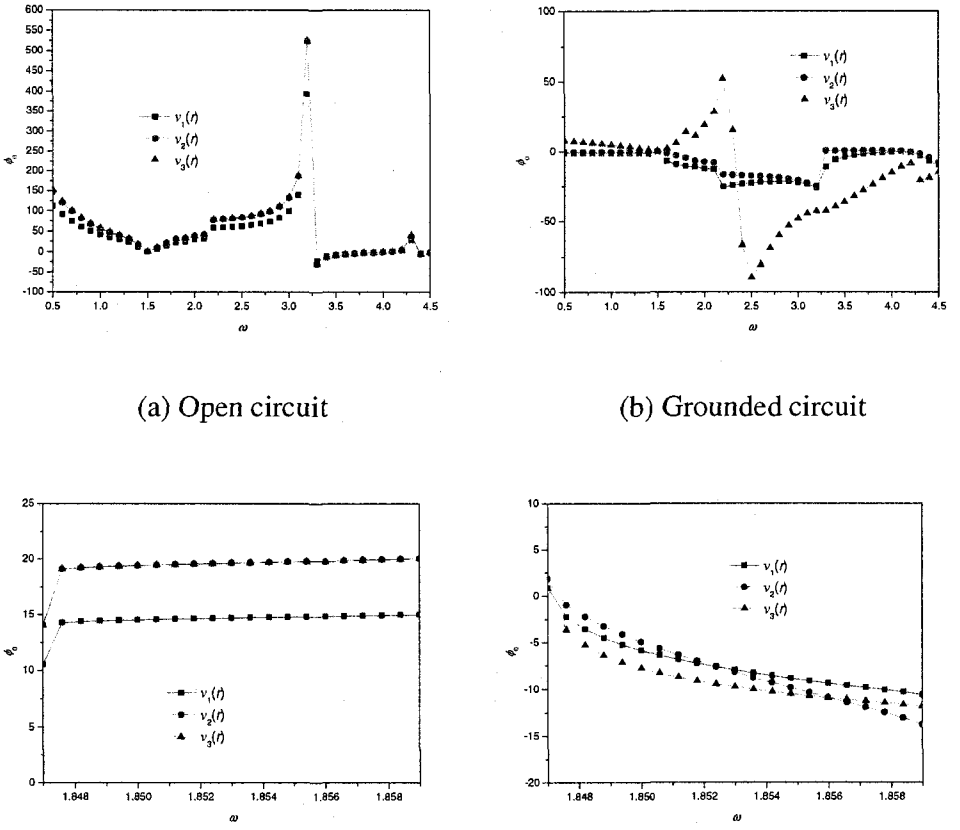

(a) Open circuit (b) Grounded circuit

(c) Open circuit in $1.847 < \omega < 1.859$ (d) Grounded circuit in $1.847 < \omega < 1.859$

Figure 17. Magnitudes of applied voltage for different voltage distributions

Thick cylinder with piezoelectric patch for $m = 1$

Case 4(A). End reflection and energy distribution for L = 0.1

In case 4(A), energy distributions and wave reflection coefficients due to an incident wave are investigated in Figure 18. The incident wave is taken as the first axisymmetric wave. The circumferential wave number is considered as $m = 1$. The electric boundary condition in the end of piezoelectric patch and the interface are open circuits ($D_z = 0$).

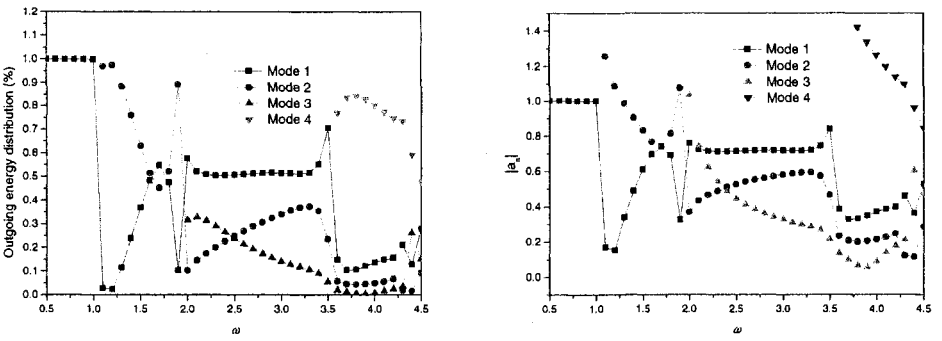

(a) (b)

Figure 18. Energy distribution and reflected coefficients

At the frequency range of interested $0.5< \omega < 1.0$, only one propagating wave exists and occupies the whole outgoing energy. When $1.1< \omega < 1.9$ two propagating waves occupy the whole outgoing energy; when $2.0 < \omega< 3.5$ three propagating waves exist; when $3.6 < \omega< 4.5$ four propagating waves share the outgoing energy and the 4th mode is the dominant mode.

Case 4(B). End reflection and energy harvest for L = 0.1 with applied voltage

Energy harvest is investigated for and the applied voltage distribution is given by

$$v(r)=\begin{cases}-1 & 0.5\le r\le 1.0\\ 1 & 1.0\le r\le 1.5\end{cases}. \tag{3.37}$$

Other parameters are same as case 4(A).

Different electric boundary conditions at the interface, namely the open circuit $D_z = 0$ and the grounded circuit $\phi = 0$, are studied.

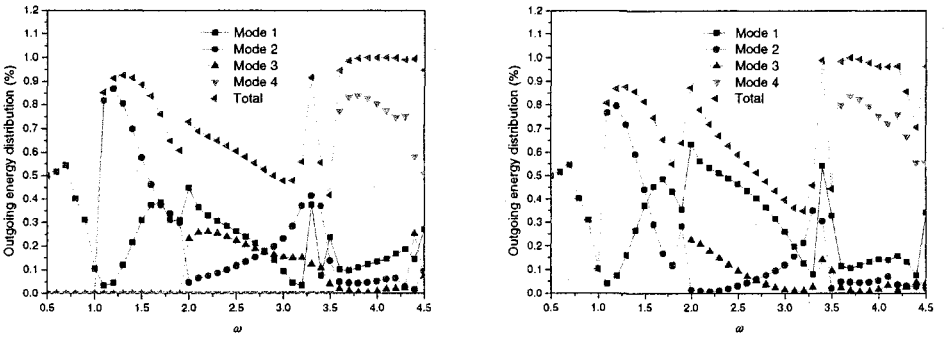

(a) Open circuit (b) Grounded circuit

Figure 19. Energy distribution for $m = 1$

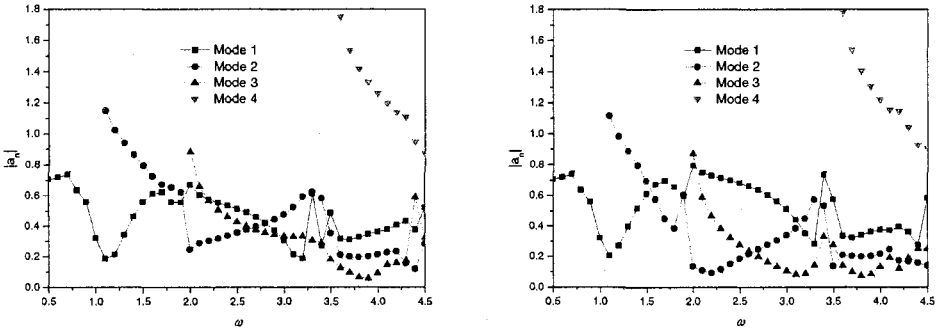

(a) Open circuit (b) Grounded circuit

Figure 20. Reflection coefficients for $m = 1$

Figure 20(a) and (b) show the reflection coefficients of the open and grounded circuit boundary conditions, respectively. On the other hand, the outgoing energy distributions for the two boundary conditions are shown in Figure 19(a) and (b).

It can be seen from Figure 19(a), at the frequency range of $0.5 < \omega < 1.0$, only one propagating wave carries outgoing energy. The propagating wave is minimized to realize relatively low outgoing energy. The maximum and minimum of outgoing energy distributions are 56.56% and 10.48%, respectively at $\omega = 0.7$ and $\omega = 1.0$, in the frequency range of $0.5 < \omega < 1.0$. When $1.1 < \omega < 1.9$ two propagating waves occupy outgoing energy; when $1.1 < \omega < 1.6$ the outgoing energy is above 80%; when $2.0 < \omega < 3.5$ three propagating waves share the outgoing energy and the energy carried

by the first propagating mode decreases largely; when 3.6< ω <4.5 four propagating waves share the outgoing energy and the outgoing energy keeps relatively high and almost constant value (above 94.5%).

In Figure 19(b), the behavior of the outgoing energy for the grounded circuit condition as shown is similar to that of the open circuit. At ω = 2.0 the outgoing energy in the grounded circuit is 87.42% compared with 73.02% in the open circuit. At ω = 3.3 and 3.4, the outgoing energy distributions in the grounded circuit are 55.67% and 98.96% compared with 91.76% and 45.97% in the open circuit. At ω = 4.4, the outgoing energy in the grounded circuit is 70.65% compared with 99.40% in the open circuit.

Case 5. Effects for different thickness of the patch on the energy harvest

Four different normalized thicknesses of the patch, namely L = 0.025, 0.05, 0.075, 0.1, are used to study their effects on energy harvest. The other conditions are the same as in Case 4.

When normalized thickness of the patch varies from 0.025 to 0.1, energy distributions of reflected waves and magnitudes of applied voltage are shown in Figure 21 and Figure **22**.

In Figure 21, the difference of the minimized outgoing energy between the open and grounded circuit conditions is very limit at the range of 0.5 < ω <1.8. When 0.5< ω < 4.5 the difference of the minimized outgoing energy for different thickness patch is small in the open circuit condition. It also can be seen that the minimized outgoing energy is less sensitive to the thickness of the patch in the open circuit condition than that in the grounded circuit condition

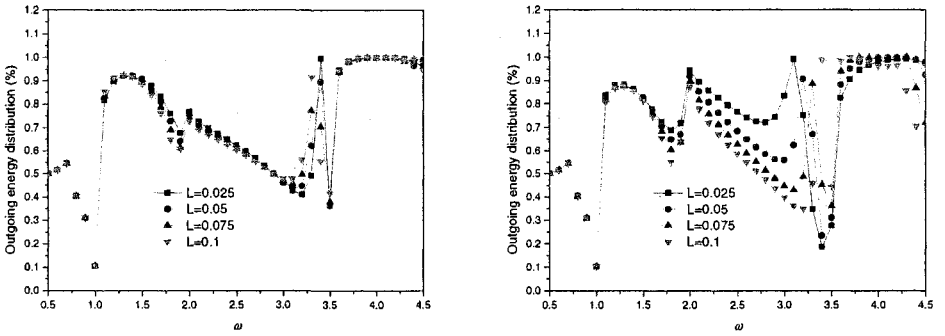

(a) Open circuit (b) Grounded circuit

Figure 21. Outgoing energy for different thickness of the patch

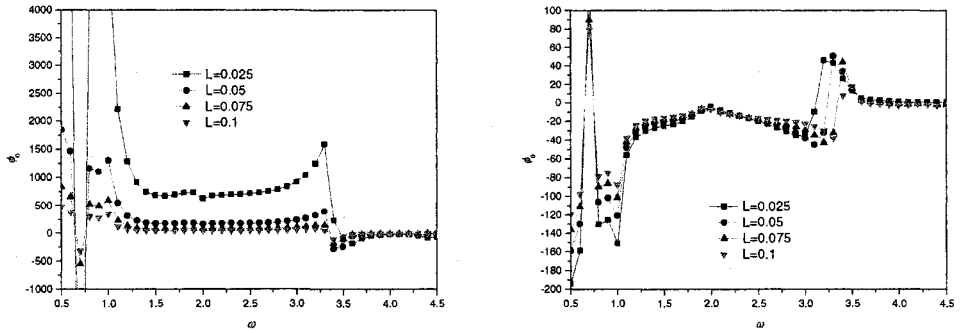

(a) Open circuit (b) Grounded circuit

Figure 22. Magnitudes of applied voltage for different thickness of the patch

As shown in Figure 21(b), in the grounded circuit condition the behaviors of the outgoing energy distributions for the different thickness patch are similar when $0.5< \omega <2.1$ and $3.7<\omega<4.5$. When $2.2< \omega<3.2$ the outgoing energy for the thicker patch is lower than that of the thinner one; when $3.2< \omega<3.7$ there is a rimple of outgoing energy for the different thickness patch.

However, as shown in Figure 14, Figure **22**(a) and (b), the applied voltages are sensitive to the thickness of the piezoelectric patch. Amplitude of the applied voltage in the thicker piezoelectric patch is much smaller than that in the thinner one. Furthermore, the magnitude of the applied voltage in the open circuit condition is hundreds times larger than that in the grounded circuit condition.

Case 6. Effects of the applied voltage on the energy harvest

In this case, effects of three different applied voltage distributions are investigated. The voltage distributions are given by

$$v_1(r)=\begin{cases}-1 & 0.5\le r\le 1.0\\ 0.5 & 1.0\le r\le 1.5\end{cases},\quad v_2(r)=\begin{cases}-1 & 0.5\le r\le 1.0\\ 1 & 1.0\le r\le 1.5\end{cases},\quad v_3(r)=\begin{cases}-0.5 & 0.5\le r\le 1.0\\ 1 & 1.0\le r\le 1.5\end{cases}. \tag{3.38}$$

The other parameters are the same as those in case 4.

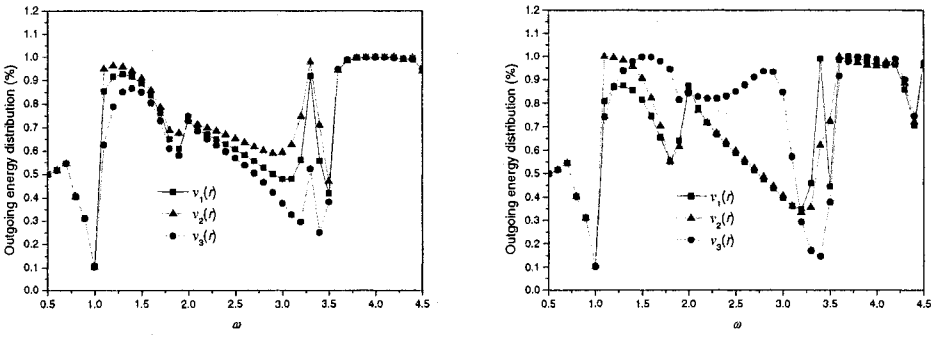

(a) Open circuit (b) Grounded circuit

Figure 23. Outgoing energy for different voltage distributions

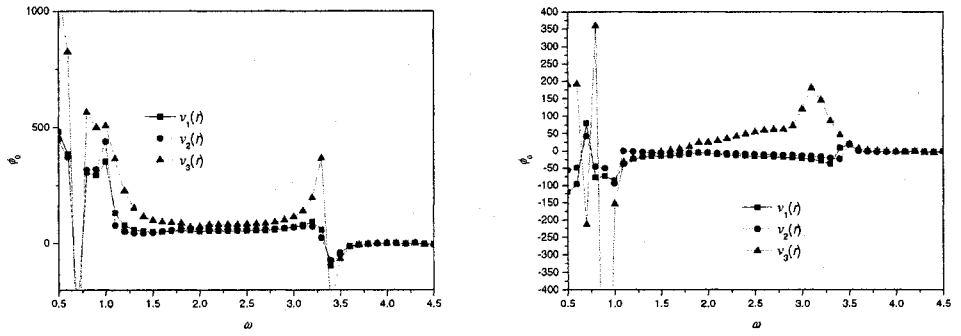

(a) Open circuit (b) Grounded circuit

Figure 24. Magnitudes of applied voltage for different voltage distributions

As shown in Figure 23(a) and Figure **24**(a), in the open circuit condition, the outgoing energy of these three voltage distributions are similar at the frequency range of $0 < \omega < 1.0$ and $3.6 < \omega < 4.5$. In the range of $1.1 < \omega < 3.5$, the outgoing energy for $v_3(r)$ is lower than that for $v_1(r)$ as the outgoing energy for $v_1(r)$ is lower than that for $v_2(r)$. The magnitudes for $v_1(r)$ and $v_2(r)$ are similar and the magnitude for $v_3(r)$ is larger than that for $v_1(r)$ and $v_2(r)$.

As shown in Figure 23(b) and Figure **24**(b), in the grounded circuit condition, outgoing energy proportions of these three voltage distributions are the same at the range of $0 < \omega < 1.0$ and $3.6 < \omega < 4.5$. The obvious difference of the outgoing energy for $v_1(r)$, $v_2(r)$ and $v_3(r)$ takes place at the frequency range of $1.1 < \omega < 3.5$. When $1.1 < \omega < 3.3$ the outgoing energy for $v_3(r)$ is higher than that for $v_1(r)$ and $v_2(r)$; when $3.4 < \omega < 3.5$ the outgoing energy for $v_3(r)$ is lower than that for $v_1(r)$ and $v_2(r)$.

However, the magnitude for $v_3(r)$ is higher than that for $v_1(r)$ and $v_2(r)$ in the frequency range of $1.6 < \omega < 3.5$.

Thin cylinder with piezoelectric patch for $m = 0$

Case 7(A). End reflection and energy distribution for L=0.1

In this case, as shown in Figure 25, energy distributions and wave reflection coefficients due to an incident wave are studied. The incident wave is taken as the first axisymmetric wave. The electric boundary conditions at the end of piezoelectric patch and the interface are open circuits ($D_z = 0$).

It can be seen that the second propagating wave occupies very low outgoing energy (below 0.167%) in the frequency range of $0.5 < \omega < 4.5$. When $0.5 < \omega < 3.1$ the whole outgoing energy is carried by the first propagating wave; when $3.1 < \omega < 3.4$ the outgoing energy carried by the first propagating wave descends to 5.22% and the outgoing energy carried by the third propagating wave jumps to 94.78%; when $3.5 < \omega < 4.5$ the outgoing energy carried by the third propagating wave keeps high value (beyond 84.05%) and the outgoing energy carried by the first propagating wave is

relatively low.

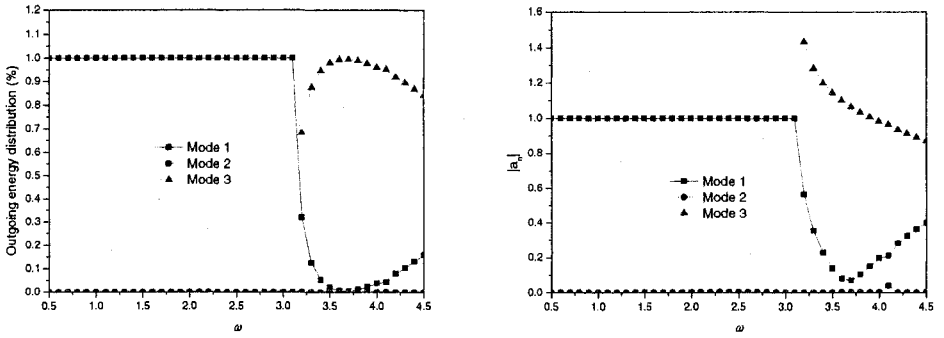

(a) (b)

Figure 25. Energy distribution and reflected coefficients

Case 7(B). End reflection and energy harvest for L=0.1 with applied voltage

Energy harvest is studied by applying appropriate voltage at the end of the piezoelectric patch. The applied voltage distribution is given by

$$v(r)=\begin{cases}-1 & 0.5\le r\le 1.0\\ 1 & 1.0\le r\le 1.5\end{cases}. \tag{3.39}$$

Other parameters are same as case 7(A).

Different electric boundary conditions at the interface, namely the open circuit ($D_z = 0$) and the grounded circuit ($\phi = 0$), are studied.

Figure 25(a) and (b) show the reflection coefficients of the open and grounded circuit boundary conditions, respectively. On the other hand, energy distributions for two different boundary conditions are shown in Figure 26.

For the open circuit condition as shown in Figure 26(a), when $0.5 < \omega < 3.1$, the outgoing energy carried by the first propagating wave is minimized efficiently. At $\omega =$ 3.1, the outgoing energy decreases to 6.89% and the outgoing energy of the first propagating wave is 5.45%, and the outgoing energy of the second propagating wave is 1.44%. In the frequency range of $3.2 < \omega < 4.5$, the outgoing energy keeps a relatively high value (beyond 87%).

For the grounded circuit condition as shown in Figure 26(b), the behavior of the outgoing energy is similar to that of the open circuit condition when $0.5< \omega <3.1$. In the frequency range of $3.2< \omega <4.5$, the outgoing energy is lower (about 91%) than that (about 99%) of the open electric condition except at $\omega = 4.0$. The outgoing energy is 97.78% compared with 99.39% in the open circuit condition at $\omega = 4.0$.

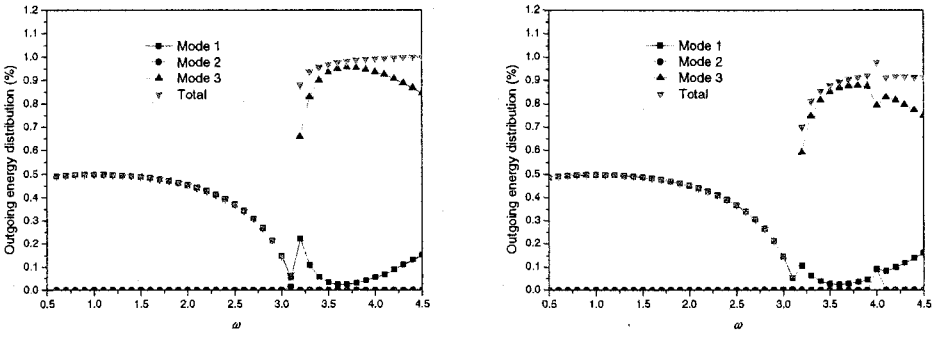

(a) Open circuit (b) Grounded circuit

Figure 26. Energy distribution for $m = 0$

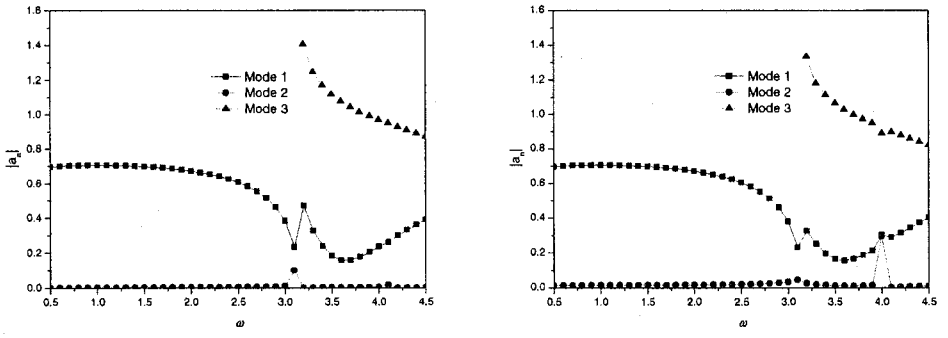

(a) Open circuit (b) Grounded circuit

Figure 27. Reflection coefficients for $m = 0$

Case 8. Effects for different thickness of the patch on the energy harvest

Four normalized different thicknesses of the patch, namely L = 0.025, 0.05, 0.075, 0.1, are used to study their effects on energy harvest. The other conditions are the same as those in case 7.

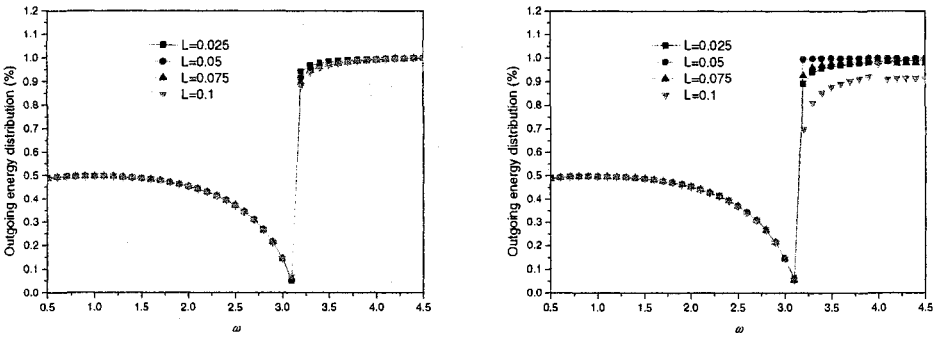

(a) Open circuit (b) Grounded circuit

Figure 28. Outgoing energy for different thickness of the patch

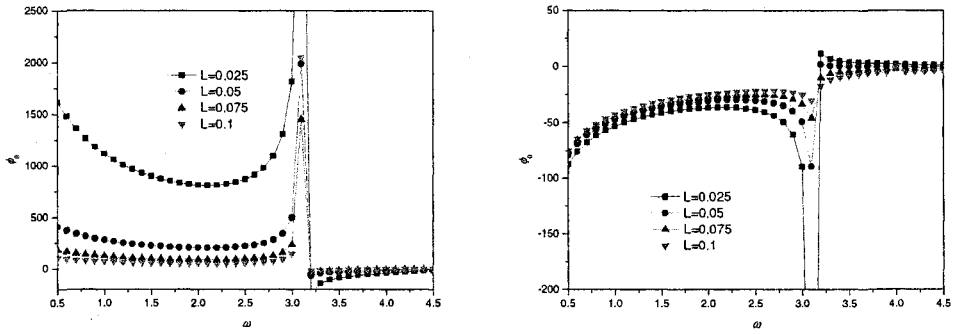

(a) Open circuit (b) Grounded circuit

Figure 29. Magnitudes of applied voltage for different thickness of the patch

When the normalized thickness of the patch varies from 0.025 to 0.1, energy distribution of reflected waves and magnitudes of applied voltage are shown in Figure 28 and Figure **29**.

In Figure 28(a) and (b), the difference of the minimized outgoing energy between the open and grounded circuit conditions is very limit except in the range of $3.1 < \omega < 4.5$. It can be seen that the minimized outgoing energy is less sensitive to the thickness of the patch in the open circuit condition than that in the grounded circuit condition.

For the grounded circuit condition, as shown in Figure 28(b), the outgoing energy distributions of different thickness of the patches are similar at the range of 0.5

$< \omega < 3.1$. At the range of $3.2 < \omega < 4.5$, the outgoing energy of the thicker patch is lower than that of the thinner one except at $\omega = 4.0$. At $\omega = 4.0$, the outgoing energy of the four sizes of the patches are close to 99%. As shown in Figure 29 (b), the lower magnitude corresponds to the thicker patch in the grounded circuit condition.

However, as shown in Figure 29 (a) and (b), the applied voltages are sensitive to the thickness of piezoelectric patch. The amplitude of the applied voltage in the thicker piezoelectric patch is much smaller than that in the thinner one. Furthermore, the magnitude of the applied voltage in the open circuit condition is hundreds times larger than that in the grounded circuit condition.

Case 9. Effects for different applied voltage distribution on the energy harvest

In this case, effects of three different distributions of the applied voltage are investigated. The three distributions are given by

$$v_1(r) = \begin{cases} -1 & 0.5 \le r \le 1.0 \\ 0.5 & 1.0 \le r \le 1.5 \end{cases} \quad v_2(r) = \begin{cases} -1 & 0.5 \le r \le 1.0 \\ 1 & 1.0 \le r \le 1.5 \end{cases} \quad v_3(r) = \begin{cases} -0.5 & 0.5 \le r \le 1.0 \\ 1 & 1.0 \le r \le 1.5 \end{cases} \tag{3.40}$$

The other parameters are the same as those in case 7.

As shown in Figure 30(a) and Figure **31**(a), in the open circuit condition, the outgoing energy distributions of the three voltage distributions are similar when $0.5 < \omega < 4.5$. The magnitudes for $v_1(r)$ and $v_3(r)$ are almost identical in this domain. The magnitude of $v_1(r)$ is larger than that of $v_2(r)$ when $0.5 < \omega < 4.5$.

For the grounded circuit condition, as shown in Figure 31(b), the outgoing energy of the three voltage distributions is similar at the range of $0.5 < \omega < 0.6$, $1.4 < \omega < 2.8$ and $\omega = 4.0$. When $0.7 < \omega < 1.3$ the outgoing energy of $v_3(r)$ has a rimple which is higher than those of $v_1(r)$ and $v_2(r)$; when $2.9 < \omega < 3.9$ the outgoing energy for $v_2(r)$ is the largest one which followed by that for $v_1(r)$, and the outgoing energy for $v_1(r)$ is followed by that for $v_3(r)$. When $4.1 < \omega < 4.5$, the outgoing energy of $v_3(r)$ is higher than that of $v_1(r)$, and the outgoing energy of $v_1(r)$ is followed by that for $v_2(r)$. As shown in Figure 30 (b), the magnitude of $v_3(r)$ is higher than those of $v_1(r)$ and $v_2(r)$ at the range of $0.5 < \omega < 4.5$.

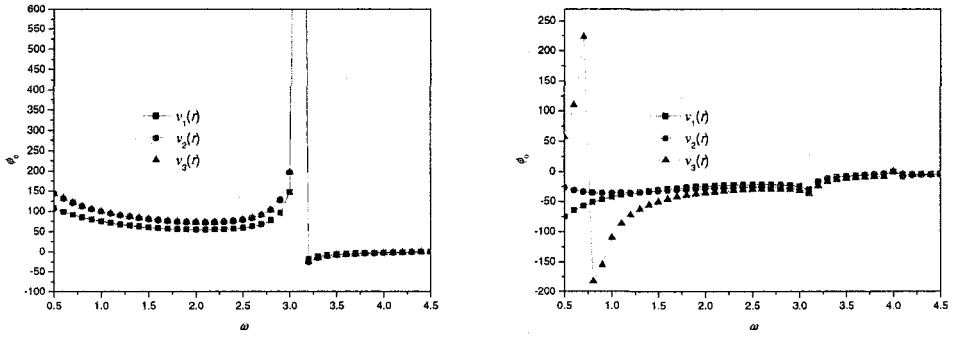

(a) Open circuit (b) Grounded circuit

Figure 30. Magnitudes of applied voltage for different voltage distributions

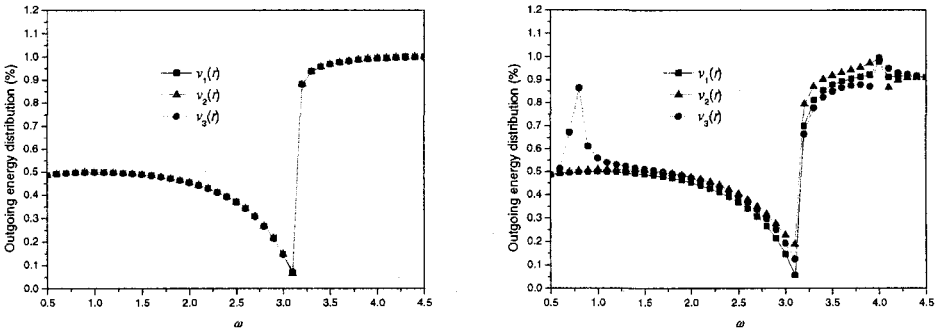

(a) Open circuit (b) Grounded circuit

Figure 31. Outgoing energy of different voltage distributions

Thin cylinder with piezoelectric patch for m = 1

Case 10(A). End reflection and energy distribution for L=0.1

In this case, shown in Figure 32, energy distributions and wave reflection coefficients due to an incident wave are studied. The incident wave is taken as the first axisymmetric wave. The electric boundary conditions at the end of piezoelectric patch and the interface are open circuits ($D_z = 0$).

It can be seen that the first propagating wave occupies major part of the

outgoing energy when 0.5< ω< 3.1. In this frequency range, the outgoing energy carried by the second and the third propagating waves are below 0.4%. When 3.2< ω< 3.7 the outgoing energy carried by the first propagating wave decreases to 0.49% and the outgoing energy carried by the fifth propagating wave increases to 97.99%; when 3.8 < ω < 4.5 the outgoing energy carried by the first propagating wave increases to 15.95% slowly and the outgoing energy carried by the fifth propagating wave descends to 83.60%.

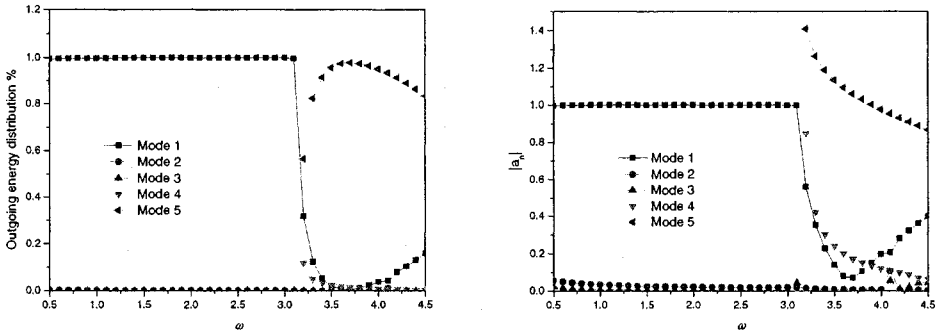

Figure 32. Energy distribution and reflected coefficients

Case 10(B). End reflection and energy harvest for L=0.1 with applied voltage

Energy harvest is studied by applying appropriate voltage at the end of the piezoelectric patch. The applied voltage distribution is given by

$$v(r)=\begin{cases}-1 & 0.5\le r\le 1.0\\ 1 & 1.0\le r\le 1.5\end{cases}. \tag{3.41}$$

Different electric boundary conditions at the interface, namely the open circuit (D_z = 0) and the grounded circuit (ϕ = 0), are studied.

Figure 34 (a) and (b) show the reflection coefficients of the open and grounded circuit boundary conditions, respectively. On the other hand, the outgoing energy carried by the outgoing wave for the two boundary conditions is shown in Figure 33(a) and 34(a). When 0.5 < ω < 3.1 the outgoing energy carried by the first propagating wave descends from 50% to 1.4%. The minimized outgoing energy is 1.44% at

$\omega = 3.1$. When $3.2 < \omega < 4.5$, the outgoing energy proportion keeps a relatively high value (beyond 88%) and increases up to 99.99% at the point $\omega = 4.5$. The outgoing energy carried by the fifth propagating wave occupies major part of the outgoing energy when $3.2 < \omega < 4.5$.

As shown in Figure 33(b), the behavior of the outgoing energy of the grounded circuit condition is the same as that of the open circuit condition when $0.5 < \omega < 3.1$. At the range of $3.2 < \omega < 4.5$, the outgoing energy of the grounded circuit is lower (about 91%) than that (about 99%) in the open circuit condition except at $\omega = 4.0$. The outgoing energy in the grounded circuit is 98.38% compared with 99.39% in the open circuit condition at $\omega = 4.0$.

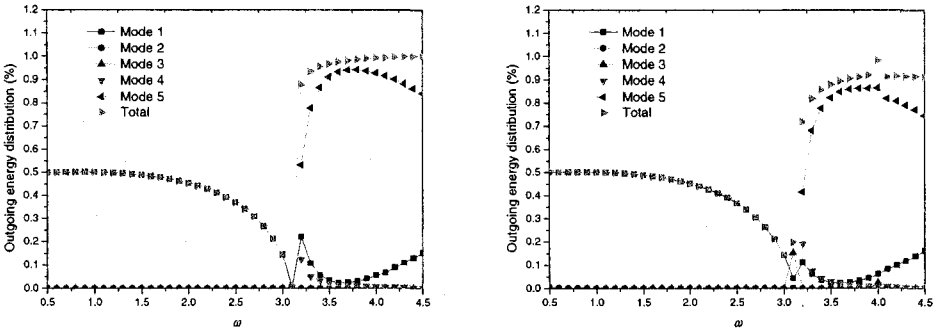

(a) Open circuit (b) Grounded circuit

Figure 33 : Energy distribution for $m = 1$

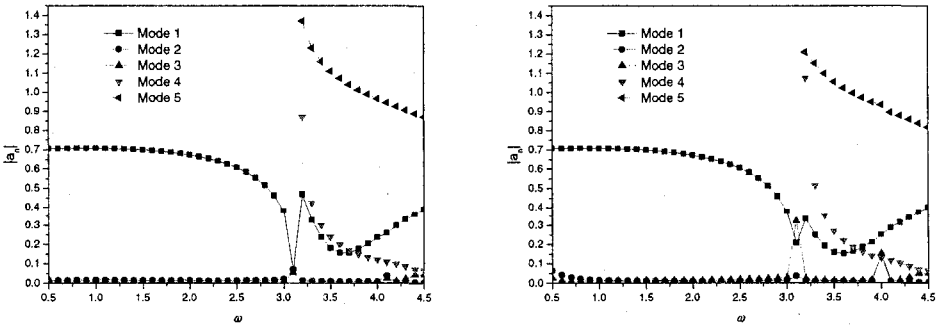

(a) Open circuit (b) Grounded circuit

Figure 34. Reflection coefficients for $m = 1$

Case 11. Effects for different thickness of the patch on energy harvest

Four normalized different thicknesses of the patch, namely L = 0.025, 0.05, 0.075, 0.1, are used to study their effects on energy harvest. The other parameters are the same as those in case 10.

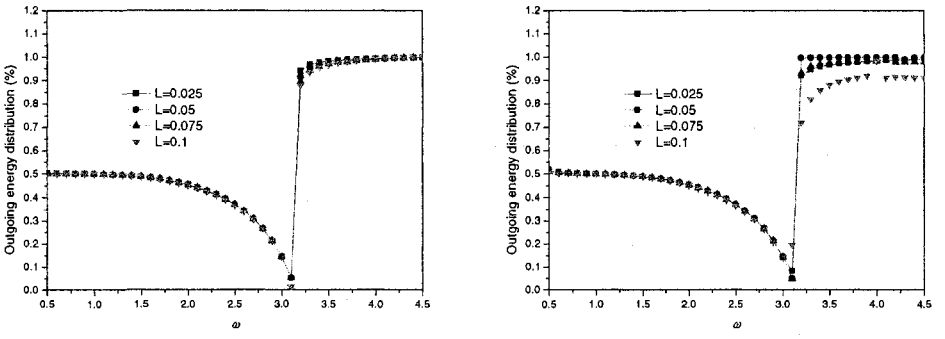

(a) Open circuit (b) Grounded circuit

Figure 35. Outgoing energy for different thickness of the patch

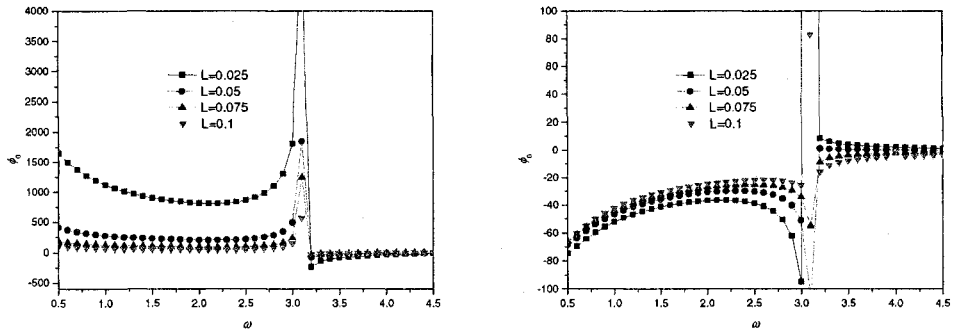

(a) Open circuit (b) Grounded circuit

Figure 36. Magnitudes of applied voltage for different thickness of the patch

When normalized thickness of the piezoelectric patch varies from 0.025 to 0.1, the energy distributions of reflected waves and magnitudes of applied voltage are

Figure 36.

In Figure 35, the difference of the minimized outgoing energy between the open and grounded circuits is very limit except at the range of $0.5 < \omega < 3.1$. It also can be seen that the minimized outgoing energy is less sensitive to the thickness of the patch in the open circuit condition than that of the grounded circuit condition.

For the open circuit condition, as shown in Figure 35(a), differences of the outgoing energy for different thicknesses of the patches are very limit when $0.5< \omega <4.5$.

For the open circuit condition, as shown in Figure 35 (b), the outgoing energy distributions of the different thicknesses of the patches are similar when $0.5< \omega <3.1$. At $\omega = 3.4$ the outgoing energy with L = 0.1 is higher (19.85%) than others. When $3.3< \omega <4.5$ the outgoing energy for the thicker patch is lower than that for the thinner one except $\omega = 4.0$. At $\omega = 4.0$, the outgoing energy distributions for four thicknesses of the patches are close to 99%. As shown in Figure 36, the lower magnitude corresponds to the thicker patch in the grounded circuit condition.

However, as shown in

Figure 36 (a) and (b), the applied voltages are sensitive to the thickness of piezoelectric patch. Amplitude of the applied voltage in the thicker piezoelectric patch is much smaller than that in the thinner one. Furthermore, the magnitude of the applied voltage in the open circuit condition is hundreds times larger than that in the grounded circuit condition.

Case 12. Effects for the applied voltage distribution on energy harvest

In this case, effects of three distributions of the applied voltage are investigated. The three distributions are given by

$$v_1(r)=\begin{cases}-1 & 0.5\le r\le 1.0\\ 0.5 & 1.0\le r\le 1.5\end{cases}\quad v_2(r)=\begin{cases}-1 & 0.5\le r\le 1.0\\ 1 & 1.0\le r\le 1.5\end{cases}\quad v_3(r)=\begin{cases}-0.5 & 0.5\le r\le 1.0\\ 1 & 1.0\le r\le 1.5\end{cases} \tag{3.42}$$

The other parameters are the same as those in case 10.

As shown in Figure 37(a) and Figure **38**(a), in the open circuit condition, the

As shown in Figure 37(a) and Figure **38**(a), in the open circuit condition, the outgoing energy for three voltage distributions are essentially the same when $0 < \omega < 4.5$ except $\omega = 3.1$. At the point $\omega = 3.1$, the outgoing energy distributions of $v_1(r)$, $v_2(r)$ and $v_3(r)$ are 1.44%, 13.29% and 4.69%, respectively.

For the grounded circuit condition as shown in Figure 37 (b), the outgoing energy for $v_3(r)$ is higher than those for $v_1(r)$ and $v_2(r)$ when $0.5 < \omega < 1.7$. At the range of $1.8 < \omega < 2.8$, the outgoing energy for $v_2(r)$ and $v_3(r)$ are contiguous and the outgoing energy for $v_1(r)$ is lower than those for $v_2(r)$ and $v_3(r)$. At $\omega = 4.0$, the outgoing energy have rimples for three distributions.

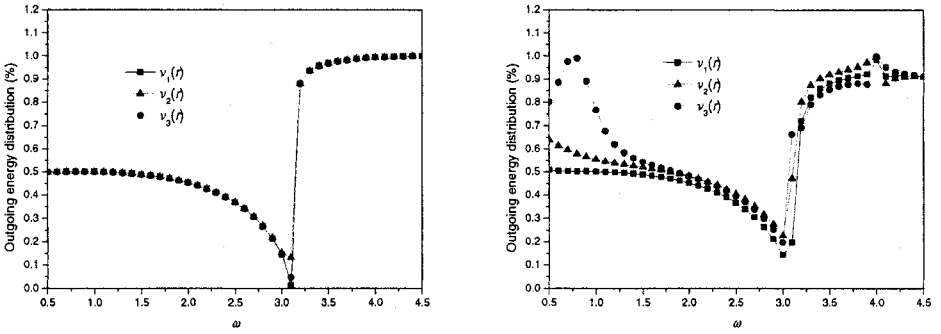

(a) Open circuit (b) Grounded circuit

Figure 37. Outgoing energy for different thickness of the patch

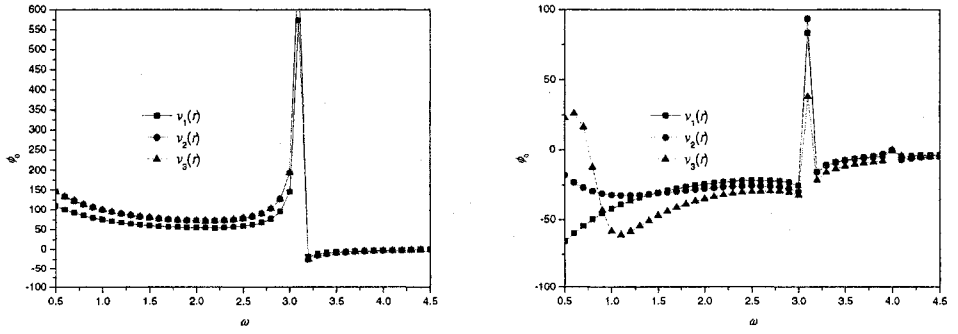

(a) Open circuit (b) Grounded circuit

Figure 38. Magnitudes of applied voltage for different thickness of the patch

3.7.2.2 End resonance

End resonance is characterized by high (but finite) amplitudes of end displacements vis-a-vis those of neighboring (i.e., slightly different) frequencies. This phenomenon is studied in this subsection.

End resonances due to the first incident axisymmetric wave are observed for a semi-infinite cylinder with/without piezoelectric patch. Both thick and thin cylinders are studied.

Results of different thicknesses of piezoelectric patches are studied. Meanwhile, the comparison of the patches with/without polarization is done to show the effect of the electric field to the end resonance. Also the results of a semi-infinite isotropic cylinder are presented for comparison purpose.

The geometry and material property of the cylinder and the patch are the same as used in case 1. The end of the piezoelectric patch is the open circuit condition (D_z = 0) and the interface of the patch and cylinder is the grounded circuit condition ($\phi = 0$).

Case 13. End resonance in the thick cylinder (H/R = 1)

As shown in Figure 39, Figure **40** and Figure **41**, there are two end resonance frequencies in the range of $0.5 < \omega < 5.0$. The first end resonance frequency takes place at a narrow range of $1.55 < \omega < 1.60$, and the second one occurs in the range of $4.0 < \omega < 5.0$. When $1.847 < \omega < 1.859$, the 'backward wave' exists and there is no end resonance performance. Detail information for these two end resonances is presented from Figure 42 to Figure 47.

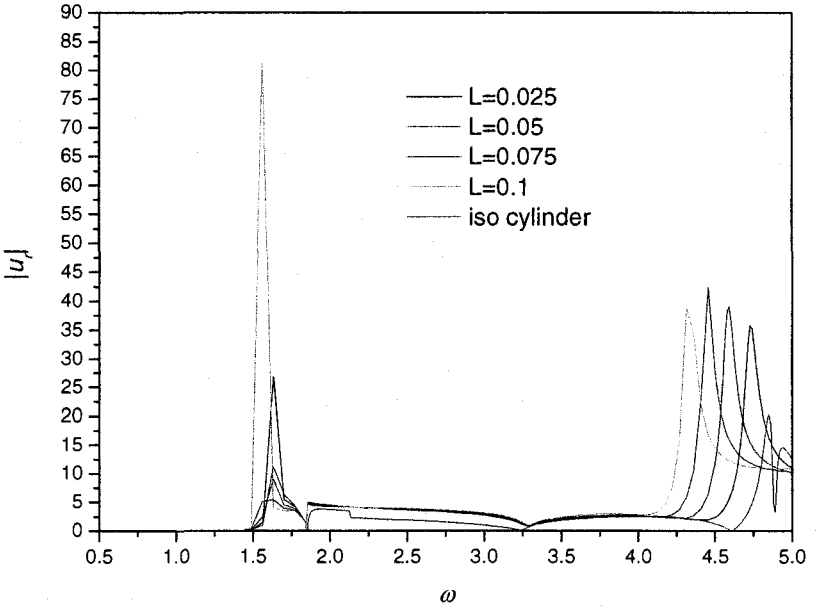

Figure 39. End resonance of radial displacement for $m = 0$

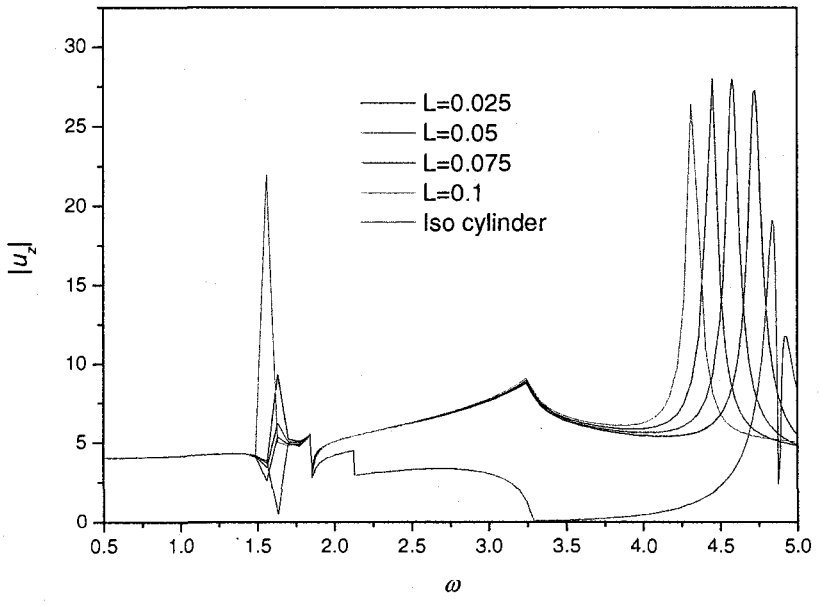

Figure 40. End resonance of axial displacement for $m = 0$

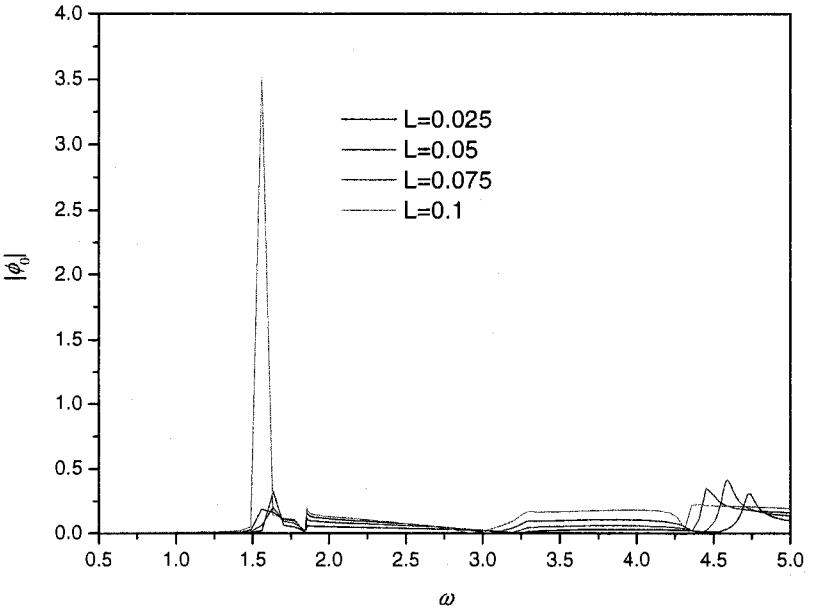

Figure 41. End resonance of electric potential for $m = 0$

The first end resonance of the thick cylinder

For the thick cylinder, as shown in Figure 42 through Figure 44, the first end resonance frequency ω decreases with the increasing thickness of the piezoelectric patch. However, the amplitude of the response increases with the increasing of the thickness of the patch.

As shown in Figure 42, the first radial end resonance frequencies are 1.6274, 1.6062, 1.5847 and 1.5626 for L = 0.025, 0.05, 0.075 and 0.1, respectively. There are slightly changes in the end resonance frequency when exploring the axial displacement and the electric potential. Table 5 summarized the results.

Table 5. First end resonance frequency for a thick cylinder

Thickness	0.025		0.050		0.075		0.100	
Patch	P[1]	NP[2]	P[1]	NP[2]	P[1]	NP[2]	P[1]	NP[2]
Radial	1.6274	1.6254	1.6062	1.6012	1.5847	1.5773	1.5626	1.5525
Axial	1.6303	1.6284	1.6075	1.6026	1.5847	1.5778	1.5634	1.5525
Electric	1.6274	NA	1.6062	NA	1.5847	NA	1.5626	NA

1: P stands for polarized piezoelectric patch

2: NP stands for non-polarized piezoelectric patch

Comparing non-polarized piezoelectric patch with polarized piezoelectric patch the first end resonance frequency shifts leftward, and the magnitude of the response increases slightly.

It can be seen from Figure 42 through Figure 44, the amplitude of the response increases monotonously with the increasing thickness of the patch.

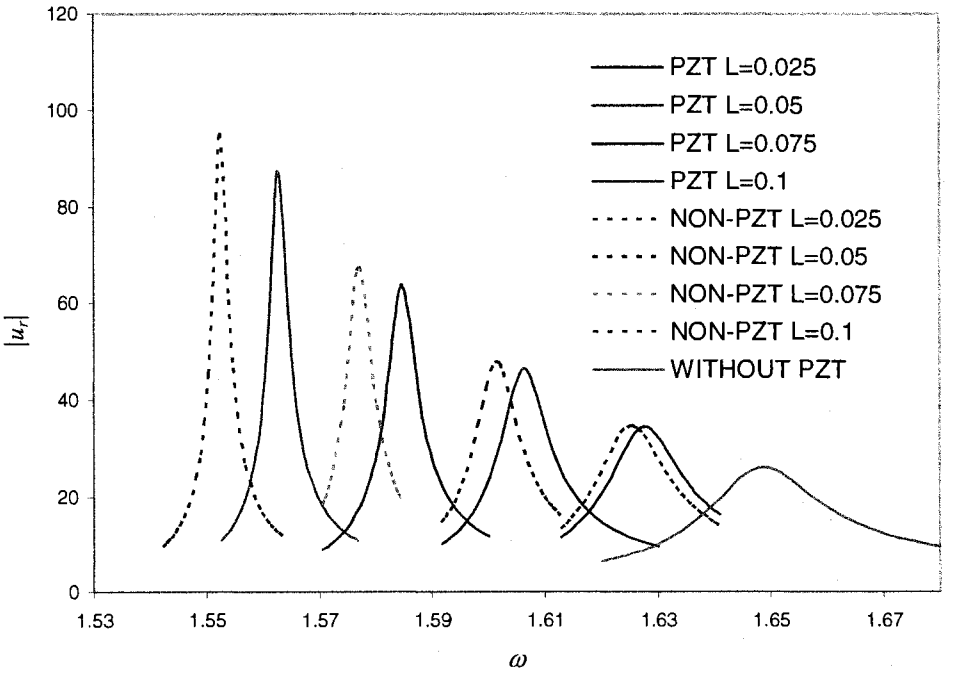

Figure 42. The first end resonance of radial displacement

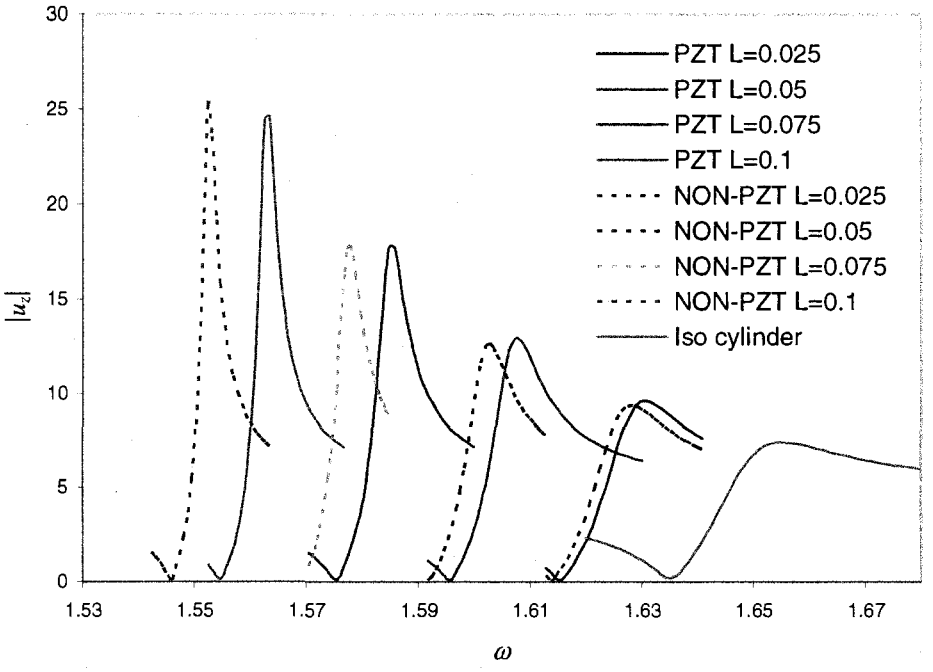

Figure 43. The first end resonance of axial displacement

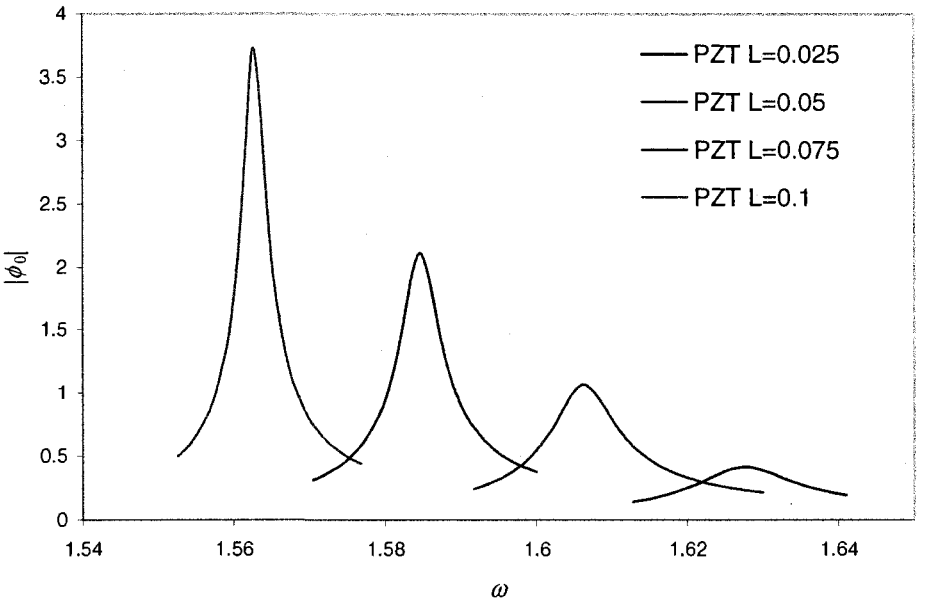

Figure 44. The first end resonance of electric potential

The second end resonance of the thick cylinder

The behavior of the second end resonance frequency is similar to that of the first end resonance frequency, i.e., it decreases with the increasing thickness of the patch. It can be seen from Figure 45 through Figure 47. However, the amplitudes of the mechanical displacements show somewhat slight variations. They are smaller than those of the first radial end resonance frequency. Table 6 summarizes the second end resonance frequency of the different thicknesses of the patches.

Table 6. Second end resonance frequency for a thick cylinder

Thickness	0.025		0.050		0.075		0.100	
Patch	P[1]	NP[2]	P[1]	NP[2]	P[1]	NP[2]	P[1]	NP[2]
Radial	4.7318	4.7135	4.5892	4.5488	4.4529	4.3876	4.3286	4.2433
Axial	4.7245	4.7061	4.5802	4.5398	4.4488	4.3835	4.3241	4.2388
Electric	4.7318	NA	4.5892	NA	4.4610	NA	4.3821	NA

1: P stands for polarized piezoelectric patch

2: NP stands for non-polarized piezoelectric patch

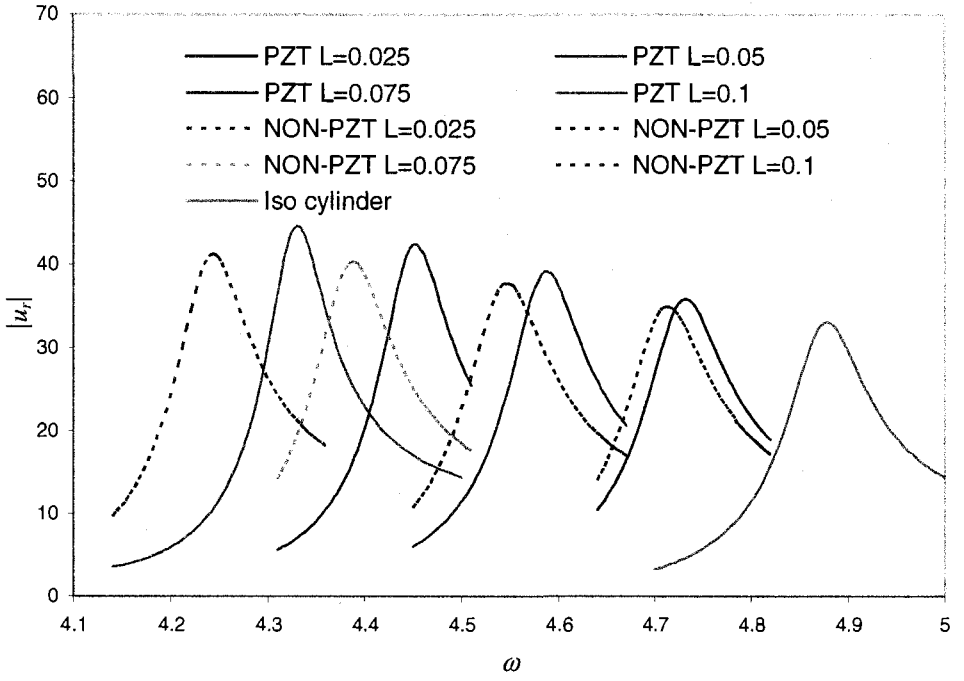

Figure 45. The second end resonance of radial displacement

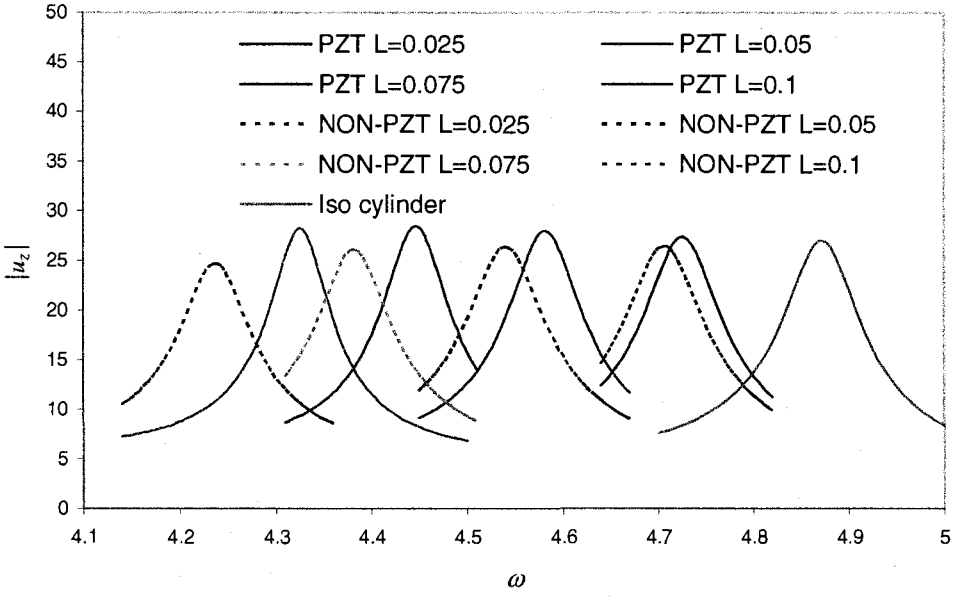

Figure 46. The second end resonance of axial displacement

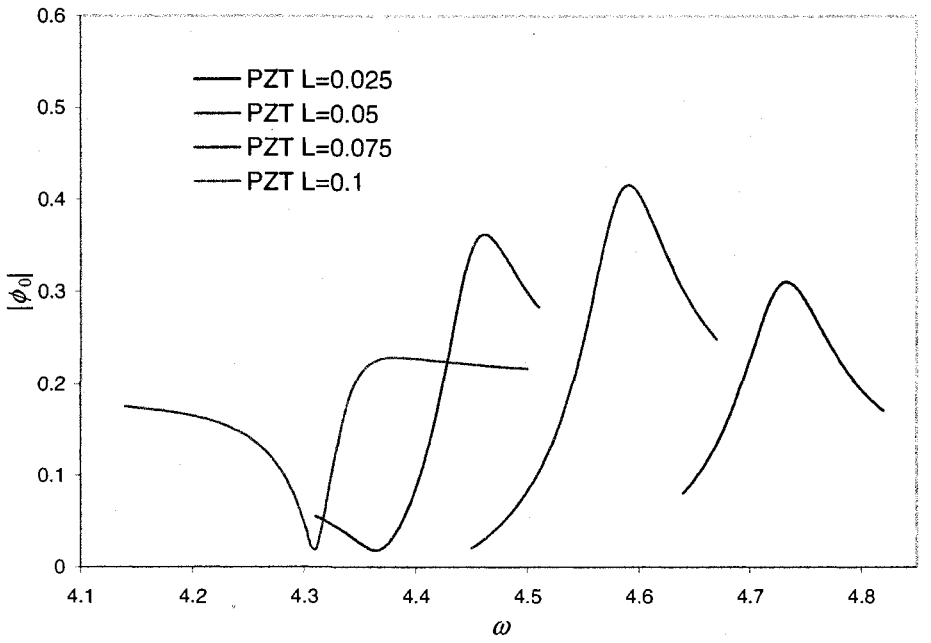

Figure 47. The second end resonance of electric potential

Case 14. End resonance in the thin cylinder (H/R = 0.135)

There is one end resonance frequency in the frequency range of interest $0.5< \omega <4.5$. As shown in Figure 48, Figure **49** and Figure **50**, the end resonance frequency ω decreases with the increasing of the thicknesses of piezoelectric patches. The end resonance frequencies of radial, nodal displacements and electric potential are similar. The amplitudes of radial and axial displacements of the end resonance show some changes with different thicknesses of the patches. However, with the increasing thicknesses of the patches the amplitudes of the electric potential increase monotonously. Table 7 summarizes the results.

Table 7. Second end resonance frequency for a thin cylinder

Thickness	0.025	0.050	0.075	0.100
Frequency	4.4673	4.3360	4.2100	4.0960
Radial amplitude	209.34	166.64	167.69	199.19
Axial amplitude	173.90	126.05	127.36	143.03
Electric amplitude	0.478	1.564	3.430	6.566

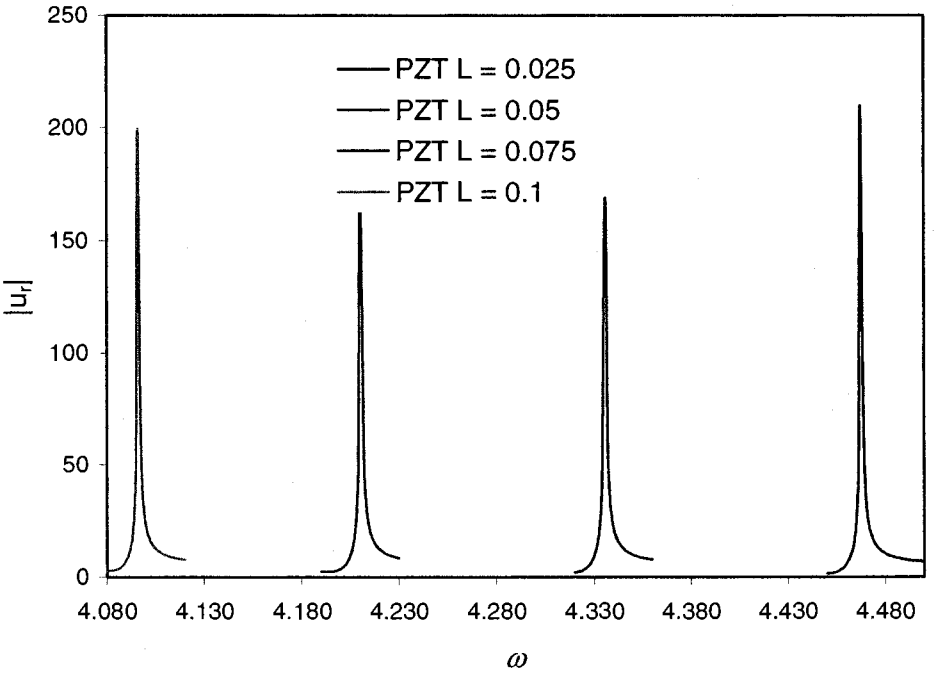

Figure 48. End resonance of radial displacement for the thin cylinder

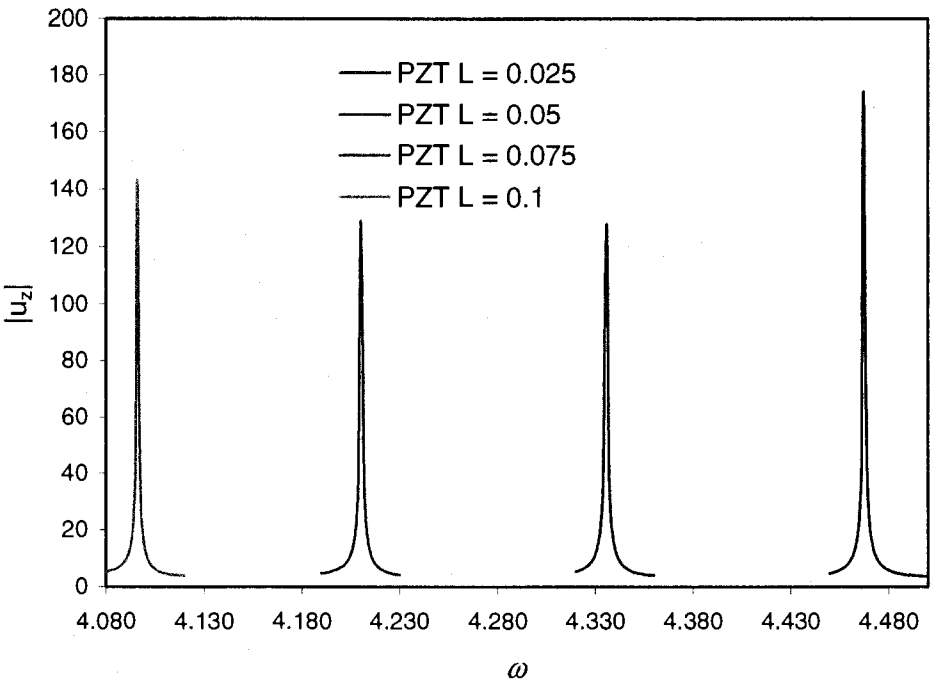

Figure 49. End resonance of radial displacement for the thin cylinder

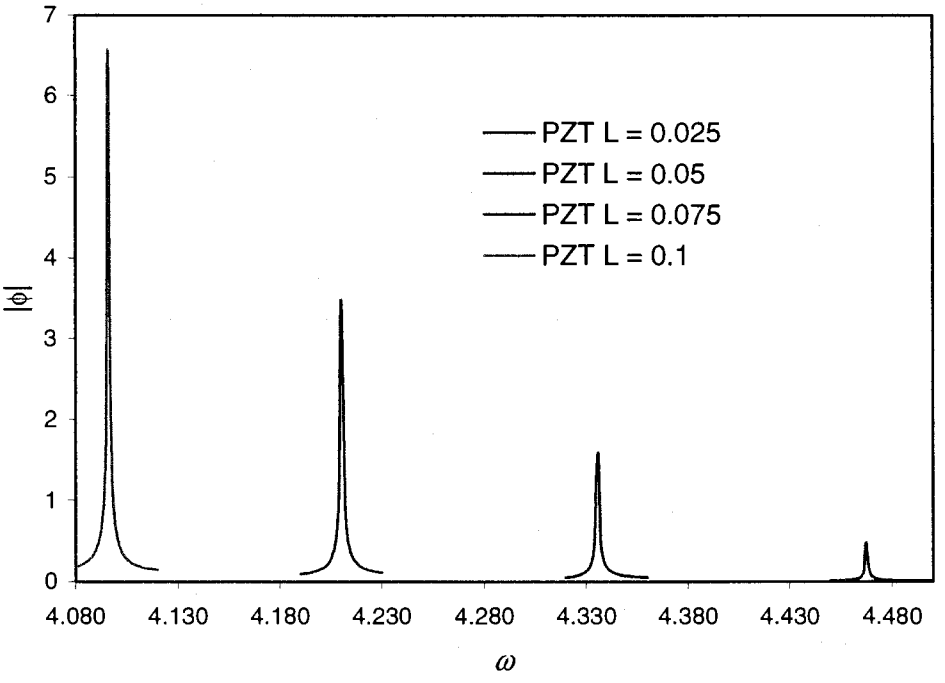

Figure 50. Resonance of electric potential for the thin cylinder

Chapter 4

Conclusions and Recommendations

4.1 Conclusions

The wave propagation and reflection in a semi-infinitely long cylinder attached with piezoelectric patch were studied in this thesis.

First, the frequency spectra of thick and thin isotropic cylinders were investigated by using the semi-analytic finite element method. Different circumferential wave numbers (m = 0 and m = 1) were considered and 'backward waves' were found in certain range of normalized circular frequency when m = 0. The wave modes were then obtained by solving the second kind of eigenvalue problem. These modes were investigated in the second part of the study.

Second, a hybrid method was introduced. In this method, the patch was modeled by two dimensional axisymmtric finite elements, and the wave in the cylinder was calculated by using a wave function expansion. The continuity conditions at the interface between the patch and cylinder were enforced. The governing equations of the system were derived by using the virtual work principle and the least square method. Finally, the reflection coefficient of the reflected field in the cylinder as well as the mechanical displacements and the electric potential in the patch were evaluated by solving the equations of motion.

The effect of the piezoelectric patch and the applied end voltage on the energy harvest and end resonance was investigated. Also studied was the electric boundary condition of the patch, namely, open circuit (D_z = 0) and grounded circuit (ϕ = 0). In

the frequency range studied, the harvested energy was insensitive to the thickness of the piezoelectric patch and the form of the end voltage. However, the amplitude of the applied end voltage was sensitive to the thickness, the form of the voltage, and the electric boundary condition. Generally speaking, the open circuit required much more effort to archive the similar amount of harvested energy than that of the grounded circuit condition. The required end voltage decreased with the increasing thickness of the patch. These observations were helpful for designing an experiment to test the energy harvest.

For the end resonance, thick and thin cylinders had different behavior. There were two end resonance frequencies existing in the thick cylinder. This was the first time that was reported in the literature, to the author's best knowledge. When the thickness of the patch increased, the end resonance frequencies decreased. Comparing polarized piezoelectric patch with non-polarized patch, it was seen that the end resonance frequencies decreased when it was polarized. The piezoelectric patch softens the structure.

4.2 Recommendations

The following recommendations are suggested for future work.

1. The end reflection results given in Chapter 3 should be validated experimentally.
2. The current program works for the two dimensional axisymmetric element. An extension to the three dimensional finite element is needed when using a generalized piezoelectric patch.
3. A more thorough study should be conducted to maximize the harvested energy or to eliminate the end resonance. Some work has been done toward this direction and the results are promising.
4. The thermal effect should be included in the future study where thermal effect becomes significant.

Appendix

$$[L]=\begin{bmatrix} \frac{\partial}{\partial r} & 0 & 0 & 0 \\ \frac{1}{r} & \frac{1}{r}\frac{\partial}{\partial \theta} & 0 & 0 \\ 0 & 0 & \frac{\partial}{\partial z} & 0 \\ 0 & \frac{\partial}{\partial z} & \frac{1}{r}\frac{\partial}{\partial \theta} & 0 \\ \frac{\partial}{\partial z} & 0 & \frac{\partial}{\partial r} & 0 \\ \frac{1}{r}\frac{\partial}{\partial \theta} & \frac{\partial}{\partial r}-\frac{1}{r} & 0 & 0 \\ 0 & 0 & 0 & -\frac{\partial}{\partial r} \\ 0 & 0 & 0 & -\frac{1}{r}\frac{\partial}{\partial \theta} \\ 0 & 0 & 0 & -\frac{\partial}{\partial z} \end{bmatrix},$$

$$[L_r]=\begin{bmatrix} \frac{\partial}{\partial r} & 0 & 0 & 0 \\ \frac{1}{r} & 0 & 0 & 0 \\ 0 & 0 & 0 & 0 \\ 0 & 0 & 0 & 0 \\ 0 & 0 & \frac{\partial}{\partial r} & 0 \\ 0 & \frac{\partial}{\partial r}-\frac{1}{r} & 0 & 0 \\ 0 & 0 & 0 & -\frac{\partial}{\partial r} \\ 0 & 0 & 0 & 0 \\ 0 & 0 & 0 & 0 \end{bmatrix}, \quad [L_\theta]=\begin{bmatrix} 0 & 0 & 0 & 0 \\ 0 & \frac{1}{r}\frac{\partial}{\partial \theta} & 0 & 0 \\ 0 & 0 & 0 & 0 \\ 0 & 0 & \frac{1}{r}\frac{\partial}{\partial \theta} & 0 \\ 0 & 0 & 0 & 0 \\ \frac{1}{r}\frac{\partial}{\partial \theta} & 0 & 0 & 0 \\ 0 & 0 & 0 & 0 \\ 0 & 0 & 0 & -\frac{1}{r}\frac{\partial}{\partial \theta} \\ 0 & 0 & 0 & 0 \end{bmatrix},$$

$$[L_z]=\begin{bmatrix} 0 & 0 & 0 & 0 \\ 0 & 0 & 0 & 0 \\ 0 & 0 & \frac{\partial}{\partial z} & 0 \\ 0 & \frac{\partial}{\partial z} & 0 & 0 \\ \frac{\partial}{\partial z} & 0 & 0 & 0 \\ 0 & 0 & 0 & 0 \\ 0 & 0 & 0 & 0 \\ 0 & 0 & 0 & 0 \\ 0 & 0 & 0 & -\frac{\partial}{\partial z} \end{bmatrix}.$$

$$[B_1]=\begin{bmatrix} N_{,r} & 0 & 0 & 0 \\ \frac{1}{r}N & 0 & 0 & 0 \\ 0 & 0 & 0 & 0 \\ 0 & 0 & N_{,r} & 0 \\ 0 & N_{,r}-\frac{N}{r} & 0 & 0 \\ 0 & 0 & 0 & -N_{,r} \\ 0 & 0 & 0 & 0 \\ 0 & 0 & 0 & 0 \\ 0 & 0 & 0 & 0 \end{bmatrix}, \quad [B_2]=\begin{bmatrix} 0 & 0 & 0 & 0 \\ 0 & \frac{1}{r}N & 0 & 0 \\ 0 & 0 & 0 & 0 \\ 0 & 0 & \frac{1}{r}N & 0 \\ 0 & 0 & 0 & 0 \\ \frac{1}{r}N & 0 & 0 & 0 \\ 0 & 0 & 0 & 0 \\ 0 & 0 & 0 & -\frac{1}{r}N \\ 0 & 0 & 0 & 0 \end{bmatrix},$$

$$[B_3]=\begin{bmatrix} 0 & 0 & 0 & 0 \\ 0 & 0 & 0 & 0 \\ 0 & 0 & N & 0 \\ 0 & N & 0 & 0 \\ N & 0 & 0 & 0 \\ 0 & 0 & 0 & 0 \\ 0 & 0 & 0 & 0 \\ 0 & 0 & 0 & 0 \\ 0 & 0 & 0 & -N \end{bmatrix}.$$

$$\left[\tilde{B}_1\right]=\begin{bmatrix} N_{,r} & 0 & 0 & 0 \\ \frac{1}{r}N & 0 & 0 & 0 \\ 0 & 0 & N_{,z} & 0 \\ 0 & N_{,z} & 0 & 0 \\ N_{,z} & 0 & N_{,r} & 0 \\ 0 & N_{,r}-\frac{N}{r} & 0 & 0 \\ 0 & 0 & 0 & -N_{,r} \\ 0 & 0 & 0 & 0 \\ 0 & 0 & 0 & -N_{,z} \end{bmatrix}, \quad \left[\tilde{B}_2\right]=\begin{bmatrix} 0 & 0 & 0 & 0 \\ 0 & \frac{1}{r}N & 0 & 0 \\ 0 & 0 & 0 & 0 \\ 0 & 0 & \frac{1}{r}N & 0 \\ 0 & 0 & 0 & 0 \\ \frac{1}{r}N & 0 & 0 & 0 \\ 0 & 0 & 0 & 0 \\ 0 & 0 & 0 & -\frac{1}{r}N \\ 0 & 0 & 0 & 0 \end{bmatrix}.$$

Reference

[1] Pochhammer, L., 1876, "Ueber die Fortpflanzungsgeschwindigkeiten Schwingungen in einem Unbegrenzten Isotropen Kreiscylinder," *Zeitschrift für* Mathematik, **81**, pp. 324-336

[2] Gazis, D. C., 1959, "Three-Dimensional Investigation of the Propagation of Waves in Hollow Circular Cylinders. I. Analytical Foundation, II, Numerical Results," *Journal of the Acoustical Society of America*, **31**(5), pp, 786-794

[3] Armenàkas, A, E., Gazis, D. C. and Herrmann, G., 1969, "*Free Vibrations of Circular Cylindrical Shells*," Pergamon Press, Oxford

[4] Mirsky, I., 1964, "Axisymmetric Vibration of Orthotropic Cylinders," *Journal of the Acoustical Society of America*, **36**, pp. 2106-2122

[5] Mirsky, I., 1964, "Three-Dimensional and Shell-Theory Analysis for Axisymmetric Vibrations of Orthotropic Shells," *Journal of the Acoustical Society of America*, **39**, pp. 549-554

[6] Nowinski, J. L., 1967, "Propagation of Longitudinal Waves in Circular Cylindrically Orthotropic Bars," *ASCE Journal of Engineering for Industry*, **89**, pp. 408-412

[7] Chou, F. H. and Achenbach, J. D., 1972, "Three-Dimensional Vibration of Orthotropic Cylinders," *Journal of Engineering Mechanics*, **98**, pp. 813-822

[8] Armenàkas, A. E. and Reitz, E. S., 1973 "Propagation of Harmonic Waves in Orthotropic Circular Cylindrical Shells," *ASME Journal of Applied Mechanics*, **27**, pp. 663-668

[9] EerNisse, E. P., 1967, "Variational Method for Electroelastic Vibration Analysis," *IEEE Transactiona on Sonics and Ultrasonic,* **SU-14**, pp. 153-160

[10] Allik, H. and Hughes, T. J. R., 1970, "Finite Element Method for Piezoelectric Vibration," *International Journal of Numerical Methods in Engineering*, **2**, pp. 151-157

[11] Nelson, R. B., Dong, S. B. and Kalra, R. D., 1971, "Vibration and Waves in Laminated Orthotropic Bars," *ASCE Journal of Engineering for Industry*, **18**, pp. 429-444

[12] Huang, K. H. and Dong, S. B., 1984, "Propagating Waves and Edge Vibrations in Anisotropic Composite Cylinder," *Journal of Sound and Vibration*, **96(3)**, pp. 635-641

[13] Rattanawangcharoen, N. and Shah, A. H., 1992a, "Guided Waves in Laminated Isotropic Circular Cylinders," *Computational Mechanics*, **10**, pp. 97-105

[14] Rattanawangcharoen, N. and Shah, A. H., 1992b, "Waves Propagation in Laminated Composite Circular Cylinders," *International Journal of Solids and Structures*, **29(6)**, pp. 761-781

[15] George, R. B. and John, P. J., 1989, "Axisymmetric Vibration of Infinite

Piezoelectric Cylinders Using One-Dimensional Finite Element," *IEEE Transactions on Ultrasonics, Ferroelectrics, and Frequency Contral*, **36**, pp. 459-465

[16] George, R. B. and John, P. J., 1991, "Vibration of Infinite Piezoelectric Cylinders with Anisotropic Properties using Cylindrical Finite Elements," *IEEE Transactions on Ultrasonics, Ferroelectrics, and Frequency Contral*, **38**, pp, 291-29

[17] Oliver, J., 1957, "Elastic Wave Dispersion in a Cylindrical Rod by a Wide-Band Short-Duration Pulse Technique," *Journal of the Acoustical Society of America*, **29**, pp. 189-194

[18] McNiven, H. D., 1961, "Extensional Waves in a Semi-Infinite, Elastic Rods," *Journal of the Acoustical Society of America*, **33**, pp. 23-27

[19] Zemanek, J., 1972, "An Experimental and Theoretical Investigation of Elastic Wave Propagation in a Cylinder," *Journal of the Acoustical Society of America,* **51(1)**, pp. 265-283

[20] Naillon, M., Coursant, R. H. and Besnier. F., 1983, "Analysis of Piezoelectric Structures by a Finite Element Method," *Acta Electronica,* **25,** pp, 341-362

[21] Ostergaard, D. F. and Pawlak, T. P., 1986, "Three-dimensional Finite Elements for Analyzing Piezoelectric structures," *Transactions of the Ultrasonic Symposium, Williamsburg, Virginia*, 639-644

[22] Gregory, R. D. and Gladwell, I., 1989, "Axisymmetric Waves in a Semi-infinite Elastic Rod," *ASME Journal of Applied Mechanics*, **42**, pp. 327-337

[23] Kharouf, N. and Heyliger, P. R., 1994, "Axisymmetric Free Vibrations of Homogeneous and Laminated Piezoelectric Cylinders," *Journal of Sound and Vibration*, **174(4)**, pp. 539-561

[24] Taweel, H., Dong, S. B. and Kazic, M., 2000, "Wave Reflection from the Free End of a Cylinder with an Arbitrary Cross-Section," International Journal of Solid and Structures, **37**, pp. 1701-1726

[25] Bai, H., Shah, A. H., Dong, S. B. and Taciroglu, E., 2006, "End reflections in a layered piezoelectric circular cylinder," *International Journal of Solids and Structures*, **43**, pp. 6309-6325

[26] Umeda, M., Nakamura, K. and Ueha, S., 1996, "Analysis of Transformation of Mechanical Impact Energy to Electrical Energy Using a Piezoelectric Vibrator,"

Japanese Journal of Applied Physics, **35**,Part 1, No. 5B, pp. 3267–3273

[27] Cornwell, P. J and Goethal, J., 2005, "Enhancing Power Harvesting using a Tuned Auxiliary Structure," *Journal of intelligent material systems and structures*, 16, PP. 825-834